EFFECTS OF PHOSPHATE ON THE TRANSPORT OF *ESCHERICHIA COLI* IN SATURATED QUARTZ SAND

by

Nan Chen

A Thesis Submitted in

Partial Fulfillment of the

Requirements for the Degree of

Master of Science

in Engineering

at

The University of Wisconsin-Milwaukee

December 2012

ABSTRACT

EFFECTS OF PHOSPHATE ON THE TRANSPORT *ESCHERICHIA COLI* IN SATURATED QUARTZ SAND

by

Nan Chen

The University of Wisconsin-Milwaukee, 2012
Under the Supervision of Professor Jin Li

Bacterial deposition and survival in porous media is a crucial phenomenon in various environmental processes including bioremediation, water treatment, and pathogen contamination. The fate of bacteria in porous media may be greatly influenced by ionic strength and phosphate. Although phosphate is widespread in the natural environment, the influence of phosphate on the transport of three strains of *ESCHERICHIA COLI* O157:H7 cells in the groundwater system remains unknown.

Experiments were performed in saturated sand packed columns with and without phosphate to examine the transport of bacteria, deposition rate coefficient, interaction energy between bacteria and sand, and bacteria surface charge.

Experimental results indicate that phosphate could enhance the transport of three strains of *ESCHERICHIA COLI* O157:H7 cells under the ionic strengths varied from 10 to 100 mM. Under higher ionic strength, three strains of *ESCHERICHIA COLI* O157:H7 cells displayed lower retention in sand. According to interaction energy profiles, majority of deposition of three strains of *ESCHERICHIA COLI* O157:H7 cells in the packed-bed system occurred in the secondary energy minimum. The response of three strains of

ESCHERICHIA COLI O157:H7 cells to different phosphate concentrations and ionic strength conditions were explained by the extended DLVO (XDLVO) theory and the steric repulsion caused by extracellular macromolecules. It was concluded that phosphate could broaden the spread of three strains of *ESCHERICHIA COLI* O157:H7 cells, and potentially other types of bacterial cells, within the soil groundwater system.

TABLE OF CONTENTS

LIST OF FIGURES

LIST OF TABLES

LIST OF ABBREVIATIONS

AFM: atomic force microscopy;

CFT: classical filtration theory;

CFU: colony forming unit;

DLVO: Derjaguin, Landau, Verwey and Overbeek;

XDLVO: extended DLVO;

HPC: heterotrophic plate count;

IS: ionic strength;

LB: Luria-Bertani;

LPS: lipopolysaccharide;

OD: optical density;

PBS: phosphate buffered saline;

PV: pore volume;

SEM: scanning electron microscopy.

ACKNOWLEDGEMENTS

I would like to thank Dr. Jin Li for her guidance, insights and support throughout the entire period of this study. Without her, I would never have had the opportunity to complete this work. Dr. Li was the most amazing advisor anyone could ask for.

My appreciation also goes to Dr. Shangping Xu and Dr. Zhen He for serving on my Master committee and for providing valuable advices on this research.

Special thanks are extended to my parents for being much more supportive than I could have imagined. Even from overseas, they always listened to my research updates, and never stopped encouraging me.

1. INTRODUCTION AND LITERATURE REVIEW

1.1. Introduction

The transport, deposition and survival of bacteria in porous media are of great importance in various environmental, industrial and health contexts, such as water quality control technology, and initiation of infection, groundwater contamination and subsurface bioremediation [1-6]. Traditionally, understandings of bacteria transport and deposition behaviors are based on studies of model colloids, such as latex microspheres, which are not necessarily representative of the complex shapes and surface characteristics of bacterial cells [5, 7-11]. Studies have shown that both physical and chemical interactions have effects on colloids deposition onto porous media, such as, hydrodynamic drag, surface charge heterogeneity, bacterial cell characteristics, hydrophobicity and electrostatic repulsive forces [5-19]. The influence of these factors on colloid adhesion to media have been tested by two experimental techniques, a packed-bed column and a radial stagnation point flow system [3, 5, 20-22].

The research reported in this thesis was undertaken to elucidate the mechanisms involved in the adhesion of E. coli, a Gram-negative bacterium in porous media and to gain insight into the impact of environmental conditions on the fate of bacteria in porous media.

1.2. Objective

The goal of this study was to gain a fundamental understanding of the mechanisms controlling bacterial adhesion in aquatic systems with relevance to subsurface porous media. The specific objectives are as follows:

1. To explore the fundamental mechanisms involved in the initial stages of bacteria adhesion, and to gain insight into the extent to which bacterial surface polymers influence bacteria adhesion.
2. To test the role of phosphate on bacterial transport and deposition in porous media.

1.3. *E. coli* O157:H7 Characteristics

E.coli O157:H7 was first recognized as a pathogen in 1982 during an outbreak investigation of hemorrhagic colitis. *E.coli* O157:H7 infection can lead to hemolytic uremic syndrome, characterized by hemolytic anemia, thrombocytopenia, and renal injury [23]. Epidemiologic investigations have demonstrated that dairy cattle, especially young animals, are a principal reservoir of *E.coli* O157:H7. Farm surveys have frequently isolated verotoxin-producing *E.coli*, including serotype O157:H7, from dairy cattle. The pathogen is typically carried by healthy cattle, and isolation of sick cattle is not likely to reduce the risk of transmission; hence, control of infection among cattle is difficult [24, 25]. A recent survey of feces of dairy calves in 14 states of the United States revealed that 22% of control herds and 50% of case herds were *E.coli* O157:H7 positive [26]. Populations of *E.coli* O157:H7 ranging from $<10^2$ to 10^5 CFU/g of feces were detected in

the positive calves, and the animals were determined to intermittently shed *E.coli* O157:H7 [27]. Depending on survival of the pathogen, bovine feces containing *E.coli* O157:H7 could be an important source of reinfection of dairy herds and a possible source of contamination of the environment.

Bovine products such as undercooked ground beef and raw milk have most often been implicated in food-borne infections with *E.coli* O157:H7. There also have been reports of *E.coli* O157:H7 outbreaks associated with both drinking and recreational water. Investigations indicated that this pathogen could remain viable in water for a long period of time or that the water might be repeatedly contaminated from unknown sources [28]. Accordingly, the highly pathogenic nature of this organism demands a clear understanding of its transport and fate in subsurface environments in order to assess and mitigate the potential risk to public health.

1.4. *E. coli* O157 mutants: *rfaC*, *waaL*

Over the past several years, several groups have elucidated the chemical structure of bacterial Lipopolysacharides (LPS) [29]. LPS is composed of the hydrophobic lipid A (the component that interacts with the inner leaflet of the outer membrane), an inner and an outer core, and the repeating units of O-antigen (Figure 1)[29]. The *rfaC* cell is LPS core biosynthesis while *waaL* cell is putative LPS biosynthesis. The LPS length of *rfaC* cell is shorter than the LPS length of *waaL* cell. [3]

Bacterial adhesion to surface has typically been described as the balance between attractive and repulsive physicochemical interactions. Long-range forces that can act

over tens of nanometers, such as London-van der Waals and electrostatic interactions, have long been recognized as influencing factors for bacterial adhesion [30]. However, often only qualitative or inconsistent correlations are observed between bacterial adhesion and the van der Waals and electrostatic properties of the substrate [31, 32]. Short-range forces include steric interactions, specific ion effects, Lewis acid-base interactions, hydration forces, hydration pressure, hydrogen bonding, and the hydrophobic effect [33]. Only recently quantitative means of including non-DLVO (Derjaguin, Landau, Verwey and Overbeek) interactions in colloidal interactions have been proposed [34]. Bacterial adhesion may also involve specific interactions between complementary surfaces such as lectin-like interactions mediated by surface polymers. Techniques that average surface properties over a population of cells do not allow for the determination of the influence of localized structures.

LPS and proteins in the outer membrane of Gram-negative bacteria as well as extracellular polysaccharides for some strains are the polymers that may influence adhesion. LPS molecules are anchored to the cell outer membrane through their lipid moiety. The core region of the LPS consists of negatively charged groups, such as phosphates and carboxylic groups, which usually give the LPS its negative charge [3]. The outer polysaccharide part of the LPS is the O-antigen, which consists of 20-70 repeating units of three to five sugars and can protrude up to 30 or more nm into the cell surroundings. For Gram-negative bacteria, the O-antigen is likely responsible for polymer interactions with surfaces. Outer-membrane proteins are less likely to interact with the solid surfaces since they are hidden behind the O-antigen layer [34].

Research with mutant bacterial strains has provided some information on how LPS macromolecules affect adhesion. Williams and Fletcher isolated mutant strains of *Pseudomonas fluorescens* whose O-antigen portion of their LPS was either missing or truncated [35]. Without the O-antigen, the mutants attached more to hydrophobic polystyrene tissue culture dishes and less to hydrophilic polystyrene dishes than did the parent strain. However, the parent and mutant strains were all adhesive to sand, which suggested that multiple types of biopolymers mediate adhesion. In some cases, the presence of LPS can facilitate adhesion through the formation of hydrogen bonds. DLVO-type repulsion may be overcome when surface polymers possessing high affinities for the solid surfaces anchor the cell to a substratum across a repulsive energy barrier. The considerable strength of these short-range interactions leading to an irreversible bacterial adhesion has been suggested to originate from the formation of the hydrogen bonds [3].

Recent advances in analytical techniques allow for the characterization of biopolymers at the nano-Newton and nanometer level. Atomic force microscopy (AFM) was used to probe the adhesive interactions and biopolymer properties of various fungal and bacterial cells [36-43]. By making contact between the microbe and an AFM tip and pulling on the surface macromolecules, the physical properties of the biopolymers (elasticity, conformation) were determined [39, 41, 42] The chemical nature of microbial surfaces was determined, aided by the use of functionalized AFM probes [36].

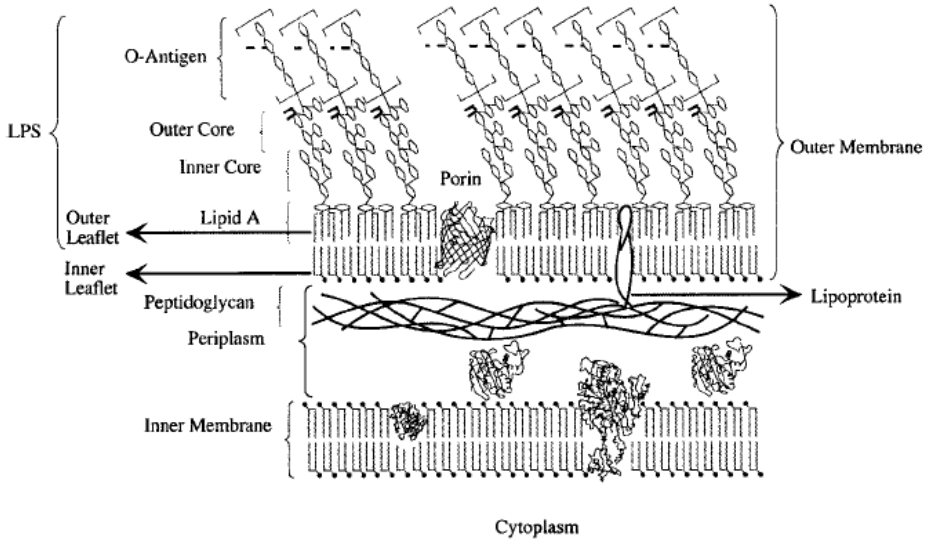

Figure 1.1 A schematic drawing of the envelope of Gram-negative bacteria. [42]

1.5. Role of Phosphate on Bacteria Transport

Previous works at both the laboratory and field scale have shown that phosphate may have an impact on the transport and the survival of bacteria in porous medium [44]. The presence of phosphate in water mains has been shown to improve the water quality by reducing the occurrence of coliform bacteria and inhibits biofilm growth, despite the fact that phosphate serves as an essential nutrient for microorganisms [45, 46].

Phosphate treatments are usually applied to water mains to control corrosion and the release of metals into the water. This procedure is highly controversial. One disadvantage of this procedure is that phosphate may serve as a nutrient for the microorganisms, which will sustain bacterial growth in waters with limited amounts of phosphate [47, 48]. However, the addition of phosphate to drinking water networks has been shown to increase the water quality by reducing biofilms, improving the efficiency

of disinfectants, decreasing the occurrence of coliforms, and surprisingly by drastically reducing bacterial production [49, 50]. These observations suggest that the favorable environment provided by the corrosion products are probably modified by the phosphate, making the environment less suitable for bacterial development.

The influence of phosphate on natural organic matter adsorption was observed by Geelhoed et al. (1998) [51]. They compared the adsorption of phosphate and citrate in single anion systems or in competitive systems and showed that phosphate has a much larger intrinsic affinity for goethite than citrate. Phosphate anions were shown to reduce citrate adsorption onto goethite significantly. Thus, similar surface sites are involved in the adsorption of both carboxyl and phosphate anions onto goethite. This competition must be responsible for the limitation of bacterial adhesion in the presence of phosphate anions. Iron oxyhydroxide surface sites, preferentially bound to phosphate anions, can no longer bind to carboxyl.

Park et al.[46] conducted packed-bed column experiments to investigate bacterial adhesion to iron-coated surfaces at various phosphate concentrations. The results showed that at phosphate concentrations between 0 and 0.5 mM, bacterial attachment to iron-coated sand decreased with increasing phosphate concentration, possible due to charge modification from positive to negative by adsorbed phosphate ions. Between 0.5 and 2.0 mM, however, bacterial attachment increased with increasing phosphate concentration, possibly due to compression of the electrical double layers between bacteria and phosphate-adsorbed/negatively charged surfaces by free phosphate ions. It

was concluded that phosphate could play different roles in bacterial interaction with iron-coated surfaces depending on its concentration.

1.6. DLVO Theory and XDLVO (extended DLVO) Theory

The standard model for bacterial adhesion implies that bacteria start from a weakly attached reversible state, where non-specific interactions are involved, and progress to a more strongly attached irreversible state, which is governed by both non-specific and specific interactions [52, 53]. The non-specific interaction energies that govern the initial phase of the bacterial adhesion mechanism are basically the Lifshitz van der Waals (LW) and the electrostatic double layer (EL) interactions, which can be either attractive or repulsive depending on the surface charge. These interaction energies are well understood and described generally in the classical DLVO theory of colloid stability [54, 55]. The DLVO theory has been widely used as a theoretical model no only qualitatively but also quantitatively to calculate the actual adhesion energy variations involved in bacterial adhesion and aggregation as a function of separation distance between the interacting surfaces [5, 20, 56, 57].

However, in the classical DLVO theory, both the substratum and the colloidal particle surfaces are assumed to be chemically inert. This is not valid for the bacterium and substratum surfaces where hydrogen and chemical bonds are involved in the adhesion mechanism. Van Oss et al. suggested an additional term called the short-range Lewis acid-base (AB) interactions to account for hydrogen bonding on close approach of bacteria and substrate surfaces, in the extended XDLVO theory [58, 59]. These AB

interactions are accounted for, in addition to LW and EL interactions, to explain the discrepancies between the DLVO predictions and experimental observations [60]. The AB interactions are based on electron acceptor/electron donor interactions between polar moieties in polar media. In addition, depending on the hydrophobic/hydrophilic property of both microbial cells and substrate surfaces, these polar interactions could be attractive (hydrophobic attraction) or repulsive (hydrophilic repulsion or hydration effects), and may be up to 10-100 orders of magnitude greater than EL and LW interactions. The addition of the polar interactions has resulted in the XDLVO approach (XDLVO) for quantifying the interaction energy in order to predict the adhesion. It as claimed that the XDLVO approach might be the promising model to explain the experimental results of bacterial adhesion since it combines both the thermodynamic approach and DLVO theory [35, 61]. However, the validation of this approach as a predictive physicochemical model to study the bacterial adhesion is still under investigation.

Many researchers have previously investigated comparison between the DLVO and XDLVO predictions. Brant et al., have investigated the investigated the interaction energies for different membrane-colloid combinations [59]. They found that the XDLVO approach predicts considerably different short-range (separation distance < 10 nm) interaction energies when compared with DLVO predictions, particularly for hydrophilic membrane-colloid combination. The hydrophilic repulsion resulted in much larger energy barrier at short-range, while the hydrophobic attraction resulted in much attractive energy profile. Meinders et al. investigated the deposition and reversibility of

bacterial adhesion on various substrate surfaces, and they have found that XDLVO model explain more accurately the bacterial adhesion than the DLVO theory for a hydrophobic substratum surface [62]. Azeredo et al. showed, on one hand, that the adhesion in phosphate buffer saline of bacterial mutants to glass is mainly explained by the DLVO theory [61]. On the other hand, they found that the XDLVO theory enabled the interpretation of the adhesion of some of these mutants to glass in presence of the exopolymers, where hydrophobic interactions played an important role in the irreversible adhesion.

1.7. Classic Colloid Filtration Theory

Colloid transport in porous media is controlled by the mass transfer of suspended particles from the bulk flow to the surface of collector grains and the attachment of particles to solid surfaces as a result of colloid-surface interaction. Yao et al. described colloid removal for water filtration in terms of two rate-limiting steps: (a) the physical processes of diffusion, interception, and gravitation setting that result in collisions between colloids and grains and (b) the chemical factors controlling the interaction forces that result in the attachment of colloid to the grain surface [63]. According to Yao's conceptual model, particle concentration in the fluid phase is represented by first order kinetics with a spatially and temporally constant colloid deposition rate coefficient. The suspended and retained particle concentrations in the porous media are therefore predicted to decrease exponentially with transport distance. Based on this assumption, the fraction of colloids recovered from the effluent of packed bed columns or aquifers is

typically used to estimate the deposition rate coefficient (K_d), or alternatively, the sticking efficiency (α) defined as the ratio of particles that attach to collector grains to particles that collide with collector grains [64].

The classical colloid filtration theory is used to determine the theoretical particle deposition distribution. This is seen through the deposition equation measuring bacteria adherence per mass of glass bead collector grain surface:

$$S(X) = \frac{t_0 \varepsilon k_d C_0}{\rho_b} \exp\left(-\frac{k_d X \varepsilon}{U}\right) \qquad (1.1)$$

where X = column depth

t_0 = injection time

ε = bed porosity

K_d = deposition rate coefficient

C_0 = initial cell concentration

ρ_b = porous medium bulk density

U = approach velocity

Deposition rate coefficients, K_d, collector removal efficiencies, η, and attachment efficiencies, α, can be computed using experimental findings and the following equations:

$$k_d = -\frac{U}{fL} \ln\left(\frac{C}{C_0}\right) \qquad (1.2)$$

where C/C_0 = normalized breakthrough concentration

U = approach (superficial) fluid velocity

f = packed bed porosity

L= length of packed bed

$$k_d = \frac{3}{2}\frac{(1-f)}{f d_c} U\eta \qquad (1.3)$$

where d_c = collector diameter

and

$$\alpha_{col} = \frac{k_d}{k_{d,fav}} \qquad (1.4)$$

In general, recent experimental successes do not coincide with the Classical Clean Bed Filtration Theory [57].

1.8. Secondary Energy Minimum

The adhesion of *E. coli* bacteria strain to quartz sand in the presence of repulsive electrostatic interactions is systematically examined. An increase in the ionic strength of pore fluid results in an increase in bacterial attachment, despite DLVO calculations indicating a sizable electrostatic energy barrier to deposition. Bacterial deposition is likely occurring in the secondary energy minimum, which DLVO calculations indicate increases in depth with ionic strength. A decrease in the ionic strength of the pore fluid

results in release of the majority of previously deposited bacteria, suggesting that these cells were deposited in the secondary minimum [57].

Redman et al. conducted a number of release experiments to investigate whether the bacterial cells retained in the packed bed during a transport experiment were indeed deposited in secondary energy minimum [57]. By numerically integrating the breakthrough curve which can demonstrate bacterial elution, Redman et al. calculated the amount of bacterial cells adhered to the quartz grains. According to these calculations, a significant fraction of the deposited bacterial cells are eluted from the column when the low ionic strength solution was introduced, ranging from an average of 0.4 when the cells were deposited in 10 mM to >0.68 when the cells were deposited at higher ionic strengths. The release of the majority of deposited cells suggests that the bacteria were not irreversibly attached to the quartz grain in a primary minimum but initially deposited within secondary energy minima.

In a study utilizing a parallel plate deposition system, Meinders et al. observed a similar behavior, where several bacterial strains attached to glass surfaces despite the very large calculated energy barriers [62]. Meinders et al. postulated that bacterial deposition occurred in the secondary energy minimum, based on a correlation between the deposition rate and the calculated secondary minimum depth.

1.9. Surface Charge

As mentioned, a great cause for bacterial adhesion to collector grain surfaces includes surface charge heterogeneity, influenced by pH of solution, zeta potential and surface

roughness of colloid and collector grain surfaces. These influences provide patches of locally favorable adhesive sites on either the colloid or collector grain surface allowing stronger adhesion in the primary energy minima [57]. Redman et al., along with other mentioned research display the use of anionic surfactants, such as sodium dodecyl sulfate or silane, during the washing process to create favorable adhesion on these repulsive patches by giving them an opposite charge. Redman's specific group also tested the transport and deposition kinetics of *E.coli* D21g on ultra pure quartz grains I packed bed columns and stagnation point flow systems using both favorable and unfavorable conditions. The tested theory shows an increase in colloid deposition on collector grain surfaces with an increase of ionic strength of buffer solution.

Redman et al., further tests the aforementioned influence of ionic strength on bacteria deposition by reducing electrostatic double layer repulsive forces by creating a more homogeneous charged surface. A depiction of the variation of DLVO interaction energy with separation distance at different ionic strengths specifically shows the depths of the primary and secondary energy minimums in Redman et al., figures. The average zeta potential in Redman's study is negative for both the colloid and collector grain surfaces. The predicted electrostatic double layer interaction energy is therefore repulsive and anticipates total cell repulsion throughout the column experiments. Despite predictions, experimental findings show a clear correlation of increasing deposition with ionic strength. Redman et al., reinforces the previous statements and details the impact that van der Waals and electrostatic double layer interaction energies have on adhesion in

the near unity linear correlation between attachment efficiency and DLVO attachment theory.

1.10. Soft Particle Theory

Claude Zobell and coworkers first introduced the importance of bacteria adhesion in the 1940s, which observed that the number of bacteria on surfaces was dramatically higher than the surrounding medium [66]. After a silent period of 30 years, the subject of bacterial adhesion again became of interest in the early 1970s. And for the last three decades, many researchers have shown great importance of elucidating the mechanisms of attachment to surfaces and understanding the influence of attachment on the bacterial cell and on the surface it attaches to.

Different from colloids, bacterial cell surfaces are highly dynamic, and respond to a variety of environmental changes. Understanding of the basic mechanisms controlling bacterial initial attachment is still lagging. Previous work on bacterial adhesion has shown that DLVO type interactions may be overcome in the presence of bacterial surface polymers, which may possess high affinities to the solid surface and anchor the cell to the surface or inhibit it by preventing the bacteria from getting close to the surface [4]. From an electrostatic perspective, bacteria must be viewed as soft particles in which ions can penetrate through the surface appendages on the cells, and thus require a fundamentally different description of surface interaction forces than for ion-impenetrable inorganic colloids [4, 67]. In addition, bacterial population heterogeneity, surface roughness, and cell motility are also known to affect bacterial adhesion.

Bacterial attachment cannot be fully understood without considering the effects of the substratum, the hydrodynamics of the aqueous medium, the characteristic of the medium, and various properties of the cell surfaces [10, 68].

1.11. Biofilm

Bacterial deposition onto biofilm-coated porous media is a crucial phenomenon in various environmental processes, including bioremediation, biofiltration, and pathogen transport in soil and groundwater [69]. Biofilm is an assemblage of microbial cells enclosed in a matrix of extracellular polymeric substances (EPS), which form on surfaces in virtually all aquatic ecosystems that can support microbial growth [6]. EPS, a complex mixture of biomacromolecules consisting primarily of polysaccharides and proteins with small but variable amounts of lipids and nucleic acids, can make up to 90% of the organic carbon in a typical biofilm. The EPS constituents contain active sites such as neutral moieties, ionized moieties and amino groups [1, 70].

The impact of biofilm EPS on bacterial adhesion is determined by a number of factors, including DLVP forces, van der Waals and electrostatic forces [71], hydrophobicity and hydration effects as described by the DLVO-AB model, and non-DLVO interactions [14]. Depending on its shape, compressibility, and chemical composition, bacterial surface EPS may encourage adhesion in porous media by polymer bridging between cells and he solid surface or hinder cells to reach the energy minimum by steric interactions. Recent atomic force microscopy (AFM) studies also have shown that interaction between biopolymer coated surfaces and bacteria are complex [72].

Biofilms are known to affect the physical and hydrodynamic properties of porous media. Different from the ion-impermeable inorganic porous media surfaces, biofilm formation provides small water channels that can help convey water and chemical solutes while preventing bacteria and colloids that are too large to pass through [73-77]. Biofilms may promote bacterial deposition by physical straining or discourage bacterial adhesion through changes in hydrodynamic conditions caused by extensive biofilm growth. As biomass accumulates, the reduced bed porosity provides an additional surface area for deposition, which can enhance particle removal [10, 78]. Conversely, reduced porosity leads to an increased local flow velocity and shear stress, which can impair the deposition.

Liu et al., demonstrated that biofilm-coated porous media might promote or impair the transport and deposition of bacteria, depending on the thickness of the biofilm and the types of EPS polymer [6]. With thin biofilm accumulation, polymer interaction between the biofilm surface EPS and bacteria plays a more important role in bacterial adhesion while porous media physical and hydrodynamic changes as a result of biofilm growth might become significant when biofilm accumulated to a certain thickness.

1.12. Hydrophobic Attraction

As known, aggregation of nonpolar substances in water is a consequence of minimizing their hydrophobic effect, which is the disruption of dynamic hydrogen bonds between water molecules causing losses in the translational and rotational entropy. Hence, the hydrophobic interaction, being at the molecular level responsible for such aggregation

phenomena of nonpolar molecules as the protein folding, formation of lipid bilayers and micelles, is due to neither a repulsive force between the water and the nonpolar molecules nor an attraction between the latter themselves [79].

At the macroscopic level, a distinctive attraction beyond the DLVO surface forces was revealed between atomically sooth mica surfaces hydrophobized by physically adsorbed cationic surfactants using surface force apparatus (SFA), obeying a short-range (up to 10 nm) exponential with a decay length of around 1 nm [80]. The extension of this extra attraction was found by a bimorph force sensor to be somehow higher (up to 20 nm) between glass surfaces (molten droplets) carrying adsorbed CTA^+ cations [81]. A long-range attraction decaying with the power law over 100 nm was even detected in atomic force microscope (AFM) between silica surfaces hydrophobized chemically by surface silylation [82-86].

Later on, the latter long-range attraction, measured between silylated surfaces of a silica sphere and a silica substrate was attributed to sub-micro cavities nucleating on the robust hydrophobic layers because of their roughness and/or exposition to air atmosphere before the immersion and execution of measurements in water [87]. Indeed, even a very long-range attraction was found to soften to the point of vanishing when interacting silylated surfaces experienced low-level vibrations around a mean static separation [88].

An attraction of longer range has also been detected between silica surfaces or mica surfaces whose hydrophobicity was imparted in situ by the adsorption of long-chain

cationic surfactants [89]. In this case, the introduction of air bubbles into the system and their stabilization on the surfaces may be assisted by the dissolved surfactants themselves. When a specific procedure that guaranteed the air-free surfactant solution by dissolving the surfactant under vacuum was used, however, the long-range attraction did not appear.

The uncertainty about the character of hydrophobic attraction (HA) manifested between fixed macroscopic surfaces is paralleled between freely moving, colliding and interacting particles in disperse systems. Really, an additional long-range attraction has been inferred from the analysis of surface forces at the onset of the so-called hydrophobic coagulation or flocculation of more or less polydisperse suspensions of highly charged silica particles, hydrophobized in air by the methylation procedure out of the suspensions [90]. This may, again, stem from capillary bridges of tiny gaseous nuclei connecting the particles and so enhancing the coagulation by overcoming the electrostatic repulsion [91, 92].

As to the coagulation initiated by the addition of cationic surface active agents, measurements on silica sols have been undertaken in which associations between hydrophobic tails of the surfactant molecules adsorbed from their solutions were considered to apply in the sense of the short-range hydrophobic attraction [93]. Unfortunately, although the effect of gas nucleation is expectably less tendentious at the adsorption layers of surfactants, the coagulation efficiency was evaluated without

the possibility of distinguishing the possible hydrophobic interaction from the DLVO ones in these experiments.

Generally, the exact analysis of surface forces within aggregating colloidal systems is possible by determining the absolute values of aggregation rate constants. The latter values were found to agree well with these, predicted from the DLVO theory without any fitting parameters, only for uniform polymer lattices carrying a low surface charge [94, 95]. As to the uniform colloidal metal oxides, however, the agreement could be obtained at the price of manipulating even fundamental parameters such as the particle radius, surface potential or the Hamaker constant beyond their physical limits, irrespective of whether relative or absolute rate constants were evaluated [96, 97].

1.13. Acid-Base Interactions

The physicochemical properties of the bacteria cells are as described previously are affected by and influence attachment and culture conditions. In a study testing acid and alkaline conditions, seven O157:H7 strains interacted more with acidic solvents, accepting and donating more electrons than with the alkaline opposition [60]. Rivas et al., conducted a similar hydrophobicity test to that of Li and Mclandsborough testing different strains of O157:H7. The electron donor/receptor tests proved O157:H7 strains' adhesion is stronger to chloroform than hexadecane proving that there is better electron donation than reception. To prove the importance of acid-base interactions, Rivas et al., conducted an experiment using 150 mmol/L high ionic PBS solutions to

inhibit the electrostatic interactions leaving the constant van der Waals interactions clearly display the acid-base interactions by their effect on the change of adherence.

2. MATERIAL AND METHODS

2.1. Bacteria Strains and Cell Preparation

The specific strains include *E.coli* O157:H7 (chlorampfenicol, kanamycin, rifampin), *rfaC* (kanamycin, rifampin) and *waaL* (kanamycin, rifampin), which obtained from Dr. C.H. Yang's lab in the department of Biological Sciences at the University of Wisconsin-Milwaukee. For each experiment, the stored strains were streaked onto Luria-Bertani (LB) agar plates and incubated at 37 ℃ overnight. A single colony was then transferred into 15mL LB broth and grown in a shaker incubator (New Brunswick Scientific E24) at 200rpm and 37 ℃ for 16-20 hours. Stationary-phase bacterial cells were harvested by centrifugation (Juan MR23i) at 3000 g and 4 ℃ for 10min. After the supernatant was decanted, the pellets were rinsed in appropriate electrolyte solutions. The centrifugation and re-suspension procedure was repeated twice to remove traces of growth media. A final cell concentration of approximately 10^7 colony forming units (CFU)/mL was obtained by optical density (OD) using an UV/Visible spectrophotometer (Shimadzu UV-1700) at 220 nm wavelength. Cell suspensions were kept on ice before the filtration experiment to minimize potential bacterial growth. The cell surface macromolecules were left unaltered in the suspension used in the column transport experiments. The motility of the bacteria did not change after the double mutation.

2.2. Electrolyte Solutions

Four different types of electrolyte solutions were used in this experiment. The total ionic strength of the electrolyte solutions was either 10 mM or 100 mM. The 10 mM electrolyte was prepared by dissolving 0.585 g/L NaCl in ultrapure water (Milli-Q water, Millipore Corp.). Under each inonic strength condition, the phosphate concentrations varied as 0 mM and 1 mM. The 1 mM phosphate buffered saline (PBS) was prepared by dissolving 1.093 g/L Na_2HPO_4, 0.3175 g/L $NaH_2PO_4 \cdot H_2O$ in ultrapure water. The pH of the electrolytes ranged from 7.0 to 7.2.

2.3. Granular Porous Medium

Cylindrical polycarbonate plastic columns (26 cm long, 2.54 cm internal diameter) were wet packed to a porosity of 0.344 with high-purity quartz sand (US Silica) with a size range of 0.354-0.420 mm. The high-purity quartz sand was heated by 70% nitric acid on a hotplate at 150 ℃ overnight. The sand was thoroughly rinsed with deionized water for 20 times before bathed in diluted NaOH solutions overnight. Followed by is the rinsing step discussed before. The sand cleansing process was repeated twice to remove surface iron oxide/hydroxide coatings and organic materials, as well as fine particles attached to sand surfaces.

2.4. Packed-bed Column Transport Experiments

A peristaltic pump (Cole Parmer, IL) was used to pump the solutions in a down flow mode. Prior to each experiment, the column was equilibrated by pumping at least 20

pore volumes of bacteria-free background NaCl solutions through the column at a constant approach velocity of 0.31 cm/min. The ionic strengths of the NaCl solutions were 10 mM and 100 mM. Approximately 3 pore volumes of bacteria suspension (~3×10^7 CFU/mL) were injected after switching the influent from the background electrolyte solution to the cell suspension. The column effluent was connected to flow-through quartz cells and the concentration of the bacterial cells was monitored every 30 s using a spectrophotometer (Shimadzu UV-1700) by measuring the absorbance at a wavelength of 220 nm [98, 99]. Following the bacteria injection, columns were eluted with 4 pore volumes background electrolyte solution until the absorbance of the effluent returned to zero. All experiments were performed in triplicates at room temperature (20-25℃).

2.5. Deposition of *E.coli* O157:H7, *rfaC* and *waaL* Cells

To compare quantitatively the overall deposition of the three *E. coli* strains at different solution ionic strengths, the deposition rate coefficient k_d was estimated using the steady state breakthrough concentrations of the cell according to the following equation [56, 100]:

$$k_d = -\frac{U}{\varepsilon \cdot L} In(\frac{C}{C_0}) \qquad (2.1)$$

where ε = porosity of the sand

U = specific discharge

L = length of the column

C/C_0 = normalized *breakthrough* concentration

2.6. XDLVO Interaction between *E.coli* O157:H7, *rfaC* and *waaL* Cells and Quartz Sand

The transport of bacterial cells within saturated porous media is governed by the energy interactions between bacterial cells and the surface of solid matrix. According to the XDLVO theory, the forces include the Lifshitz-van der Waals (LW) interactions, the electrostatic double layer (EDL) repulsion, and the Lewis acid-base (AB) interaction [101-103]:

$$\Phi^{Total} = \Phi^{LW} + \Phi^{EDL} + \Phi^{AB} \qquad (2.2)$$

The LW, EDL, and AB interaction energies ($\Phi^{LW}, \Phi^{EDL}, and\ \Phi^{AB}$) can be calculated using the following equations [43, 52, 53, 57, 104-107]:

$$\mathrm{A} = 24\pi h_0^2 \left(\sqrt{\gamma_b^{LW}} - \sqrt{\gamma_w^{LW}}\right)\left(\sqrt{\gamma_s^{LW}} - \sqrt{\gamma_w^{LW}}\right) \qquad (2.3)$$

$$\Phi^{EDL} = \pi\varepsilon_0\varepsilon_w a_b \left\{2\psi_b\psi_s In\left[\frac{1+exp(-kh)}{1-exp(-kh)}\right] + (\psi_b^2 + \psi_s^2) In[1 - exp(-2kh)]\right\} \qquad (2.4)$$

$$\Phi^{AB} = 2\pi a_b \lambda_w \Delta G_{h_0}^{AB} exp\left(\frac{h_0 - h}{\lambda_w}\right) \qquad (2.5)$$

$$\Delta G_{h_0}^{AB} = 2\left[\sqrt{\gamma_w^+}\left(\sqrt{\gamma_b^-} + \sqrt{\gamma_s^-} - \sqrt{\gamma_w^-}\right) + \sqrt{\gamma_w^-}\left(\sqrt{\gamma_b^+} + \sqrt{\gamma_s^-} - \sqrt{\gamma_w^-}\right) - \sqrt{\gamma_b^-\gamma_s^+} - \sqrt{\gamma_b^+\gamma_s^-}\right]$$

(2.6)

$$\Phi^{AB} = -\frac{Aa_b}{6h} \qquad (2.7)$$

where A = the Hamaker constant

a_b = equivalent radius of the bacterial cells

h = separation distance between the bacterium and sand surface

h_0= minimum equilibrium distance between the cell and sand surface (=0.157 nm)

γ^+= electron-accepting interfacial tension parameter

γ^-= electron-donating interfacial tension parameter

γ^{LW}= LW interfacial tension parameter

ε_0= dielectric permittivity of vacuum

ε_w= dielectric permittivity of water

k= inverse of Derby length

ψ_b= surface potentials of the bacterial cells

ψ_s= surface potentials of sand

λ_w= characteristic decay length of AB interactions in water (= 0.6 nm)

$\Delta G_{h_0}^{AB}$= hydrophobicity interaction free energies per unit area corresponding to h_0

γ_w^{LW} = 21.8 mJ/m^2 γ_w^+ = 25.5 mJ/m^2 γ_w^- = 25.5 mJ/m^2

γ_s^{LW} = 39.2 mJ/m^2 γ_s^+ = 1.4 mJ/m^2 γ_s^- = 7.8 mJ/m^2

Values of $\gamma^{LW}, \gamma^+, or\ \gamma^-$ for three *E. coli* strains sere determined by measuring the contact angles (θ) using three different probe liquids with known surface tension parameters [108]:

$$\gamma_i^L(1+\cos\theta) = 2\sqrt{\gamma_i^{LW}\gamma^{LW}} + 2\sqrt{\gamma_i^+\gamma^-} + 2\sqrt{\gamma_i^-\gamma^+} \qquad (2.8)$$

where the subscript i represents water ($\gamma^L = 72.8, \gamma^{LW} = 21.8\ and\ \gamma^+ = \gamma^- = 25.5\ mJ/m^2$), glycerol ($\gamma^L = 64.0, \gamma^{LW} = 34.0, \gamma^+ = 3.92\ and\ \gamma^- = 57.4\ mJ/m^2$) or diiodomethane ($\gamma^L = 50.8, \gamma^{LW} = 50.8\ and\ \gamma^+ = \gamma^- = 0\ mJ/m^2$) [108]. The contact angles were acquired with a Rame-Hart goniometer using bacterial lawns produced by filtering cells onto porous membrane [43].

2.7. Steric Interaction Between Cells and Quartz Sand

In biological systems, the classical DLVO model often failed to fully explain the bacterial transport and deposition behavior observed in experiments due to the presence of extracellular macromolecules on bacterial surface [56, 100-102]. The steric repulsion between two parallel surfaces similarly coated by macromolecules is described by the deGennes equation [109]:

$$P = \frac{kT}{s^3}\left[\left(\frac{2L}{D}\right)^{9/4} - \left(\frac{D}{2L}\right)^{3/4}\right] \quad \text{For } D < 2L \qquad \text{(Equation 2.9)}$$

where P is the pressure between the two parallel surfaces, D is the separation distance, L is the thickness of brush layer and s is the average distance between anchoring sites. For *E.coli* O157:H7, *rfaC*, and *waaL*, of the values of L is 30 nm [15], 2.4 nm, and 4.4 nm, respectively; the values of s is 2.2 nm [110], 2.2 nm, and 2.2 nm.

If one plate has the brush and the other plate is bare, $2D$ should substitute D and the pressure should be divided by 2 [72]:

$$P = \frac{1}{2}\frac{kT}{s^3}\left[\left(\frac{2L}{D}\right)^{9/4} - \left(\frac{D}{2L}\right)^{3/4}\right] \quad \text{For } D < L \qquad \text{(Equation 2.10)}$$

Integration using Derjaguin's approximation, we have the steric force expression for a sphere-plate system [109]:

$$P = \pi R\frac{kT}{s^3}\int_D^L\left[\left(\frac{L}{x}\right)^{9/4} - \left(\frac{x}{L}\right)^{3/4}\right]dx = \frac{4L}{35}\pi R\frac{kT}{s^3}\left[5\left(\frac{D}{L}\right)^{7/4} + \left(\frac{L}{D}\right)^{5/4} - 12\right] \quad \text{(Equation 2.11)}$$

The integration of F gives the steric interaction energy (Φ^{Steric}) for a sphere-plate system

$$\Phi^{Steric} = \int_D^L F(x)dx$$

$$= \frac{4}{385D}\pi R\frac{kT}{s^3}\left[-20D^3\left(\frac{D}{L}\right)^{3/4} + 308L^3\left(\frac{D}{L}\right)^{3/4} - 420DL^2 + 132D^2L\right]$$

(Equation 2.12)

2.8. *E.coli* O157:H7, *rfaC* and *waaL* Cells Characterization

1. Zeta Potential: Zeta potential values of bacteria cells and sand were used to represent surface potentials in Equation 2.5. Cell suspensions were prepared in a similar procedure, as in the column transport experiments and the quartz sand was pulverized to colloid-sized particles and then suspended in the electrolyte solutions. The electrophoretic mobility of the bacterial cells and colloidal quartz sand in each solution was then measured using a ZetaPALS analyzer (Brookhaven Instruments Corporation). The Smoluchowski equation was used to convert electrophoretic mobility values into zeta potentials.
2. Cell Size: To measure cell sizes, photos of Wild Type, *rfaC* and *waaL* suspended in various solutions were obtained using a Nikon Eclipse 50i microscope, equipped with a Photometric coolsnap ES digital camera and the MetaMorph software. The length and width of the cells were then determined using the ImageJ software and the equivalent radii of the cells were calculated as $\left(\sqrt{\frac{L_c \times W_c}{\pi}}\right)$, where L_c and W_c represent the length and width of the cell, respectively. The equivalent cell radius of *E. coli* O157:H7, *rfaC* and *waaL* were around 0.85 μm, 0.64 μm and 0.93 μm, respectively [111].
3. Contact Angles: The contact angles of water, glycerol, and diiodomethane on Wild Type, *rfaC* and *waaL* (Table 2.1) were measured by Rame-Hart instrument.

Contact Angle	θ_{water}	$\theta_{glycerol}$	$\theta_{diiodomethane}$
rfaC	47° (±0.2°)	32.3° (±1.1°)	54.8° (±0.6°)
waaL	28.1° (±0.4°)	25° (±0.9°)	48.7° (±0.5°)
Wild Type	22.1° (±0.1°)	27.0° (±1.8°)	63.0° (±0.7°)

Table 2.1 Measured contact angles of water, glycerol, and diiodomethane on Wild Type, rfaC and waaL cells.

3. Results

3.1. Breakthrough Curves of *E.coli* O157:H7, *rfaC*, and *waaL* Cells

Figure 3.1 presents the breakthrough concentrations of *waaL*. Results from the packed-bed transport experiments show that higher percentages of *waaL* cells should travel through the sand columns when the concentration of phosphate progressively increased from 0 to 1 mM, indicating that phosphate can promote the transport of *waaL* (Figure 3.1). At a constant ionic strength of 100 mM, 75.9% (±6.3%) and 51.8% (±6.2%) of the *rfaC* cells were immobilized within the sand columns for phosphate concentrations of 0 and 1 mM, respectively. At a constant ionic strength of 10 mM, 61.8% (±7.8%) and 9.6% (±0.96%) of the *waaL* cells were immobilized within the sand columns for phosphate concentrations of 0 and 1 mM, respectively.

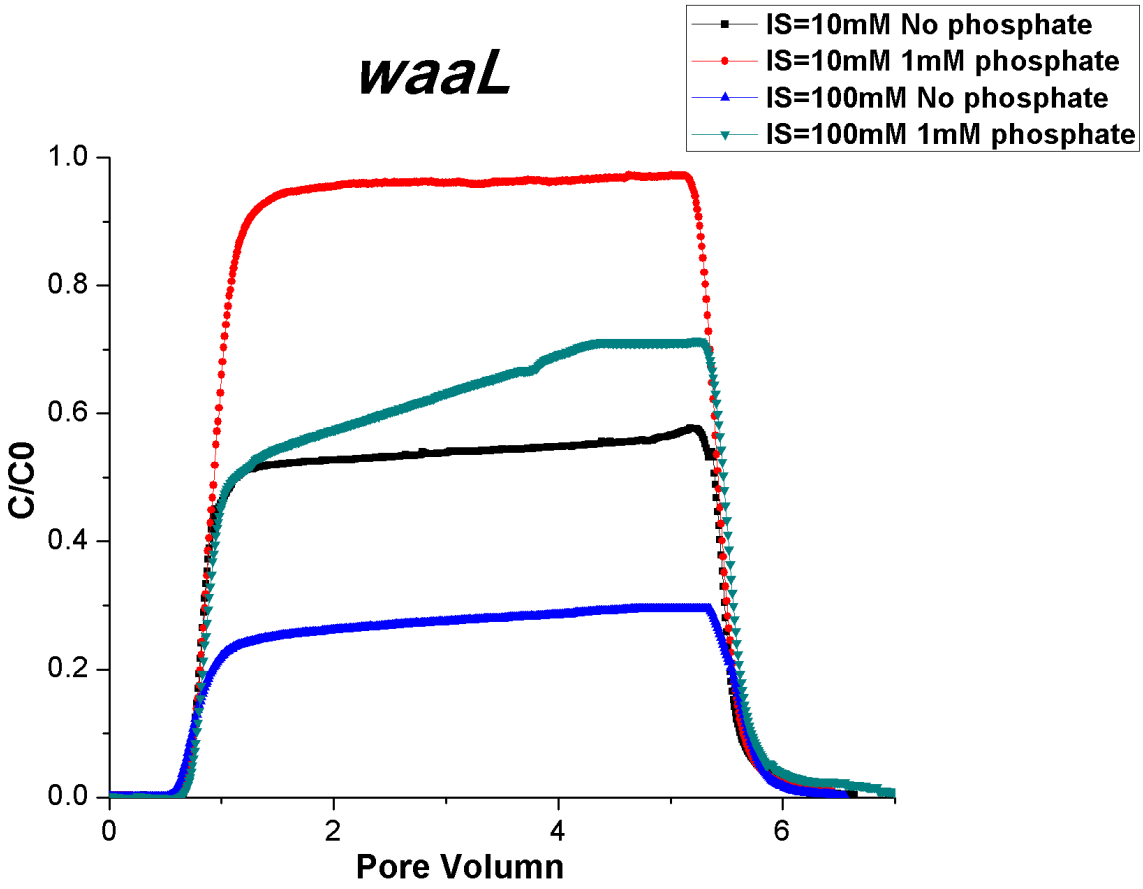

Figure 3.1 Breakthrough concentrations of waaL bacteria and saturated quartz sand, under two solution ionic strengths: 10 mM and 100 mM. Concentrations of phosphate were 0 and 1 mM. Experimental conditions were: approach velocity = 0.31 cm/min, porosity = 0.344 and pH = 7.2. Breakthrough curves represent the average of triplicate parallel packed-bed column experiments.

Figure 3.2 presents the breakthrough concentrations of *rfaC*. Results from the packed-bed transport experiments show that higher percentages of *rfaC* cells should travel through the sand columns when the concentration of phosphate progressively increased from 0 to 1 mM, indicating that phosphate can promote the transport of *rfaC* (Figure 3.2). At a constant ionic strength of 100 mM, 74.3% ($\pm$2.9%) and 41.8% ($\pm$0.027%) of

the *rfaC* cells were immobilized within the sand columns for phosphate concentrations of 0 and 1 mM, respectively. At a constant ionic strength of 10 mM, 43.3% (±4.8%) and 4.7% (±1.9%) of the *rfaC* cells were immobilized within the sand columns for phosphate concentrations of 0 and 1 mM, respectively.

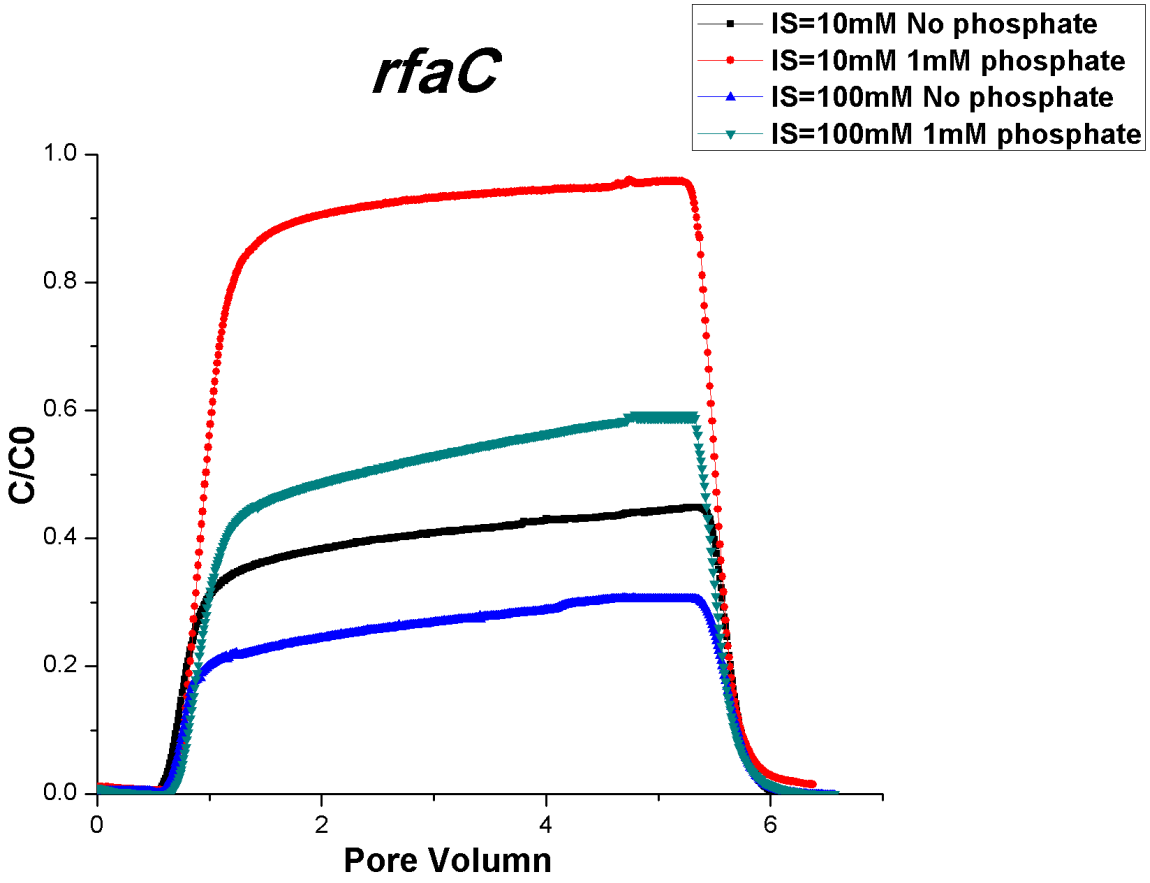

Figure 3.2 Breakthrough concentrations of rfaC bacteria and saturated quartz sand, under two solution ionic strengths: 10 mM and 100 mM. Concentrations of phosphate were 0 and 1 mM. Experimental conditions were: approach velocity = 0.31 cm/min, porosity = 0.344 and pH = 7.2. Breakthrough curves represent the average of triplicate parallel packed-bed column experiments.

Figure 3.3 presents the comparison of breakthrough curves between *E.coli* O157:H7, *rfaC*, and *waaL* cells. The breakthrough curve of *rfaC* was higher than *waaL* in the same scale under each condition, which indicated *waaL* efficient transport ability in the quartz sand.

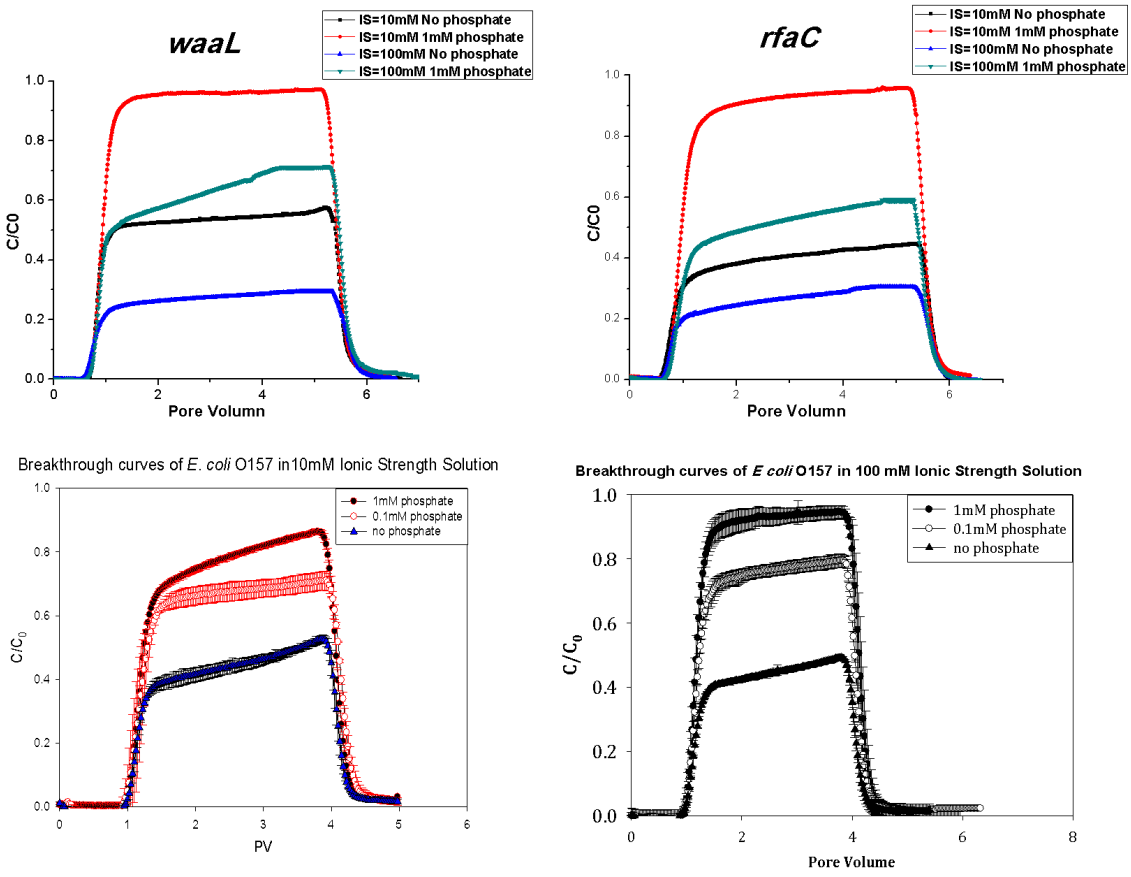

Figure 3.3 Comparison of breakthrough curves between E.coli O157:H7, rfaC, and waaL cells. Experimental conditions were: approach velocity = 0.31 cm/min, porosity = 0.344 and pH = 7.2. Breakthrough curves represent the average of triplicate parallel packed-bed column experiments.

3.2. Deposition Rate of *E.coli* O157:H7, *rfaC*, and *waaL* Cells

Figure 3.4 presents deposition rate coefficient (k_d) of *waaL* bacteria cells. At a constant ionic strength of 100 mM, deposition rate coefficient (k_d) decreased from 0.082 ($\pm$0.0066) min^{-1} to 0.033 ($\pm$0.000028) min^{-1} when phosphate concentration increased from 0 to 1 mM (Figure 3.4). A similar trend was observed when the ionic strength was maintained at 10 mM. The deposition rate coefficient decreased from 0.034 ($\pm$0.0052) min^{-1} to 0.0029 ($\pm$0.0012) min^{-1} when phosphate concentration increased from 0 to 1 mM, respectively.

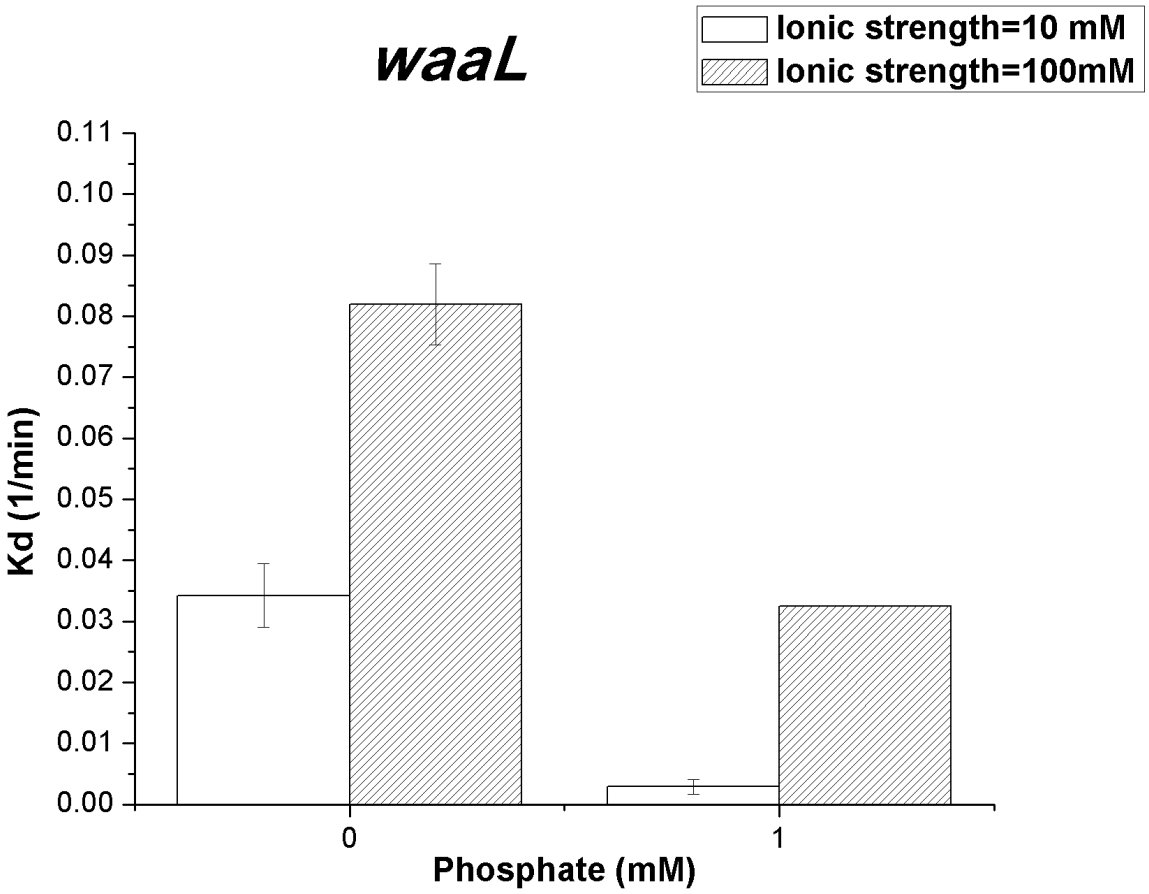

Figure 3.4 Bacteria's deposition rate coefficient (kd) of waaL cells was determined from the breakthrough curves using Equation 2.1 under both ionic strengths. Experimental conditions were: approach velocity = 0.31 cm/min, porosity = 0.344 and pH = 7.2. Error bars represent standard deviations of triplicate measurements.

Figure 3.5 presents deposition rate coefficient (k_d) of *rfaC* bacteria cells. At a constant ionic strength of 100 mM, deposition rate coefficient (k_d) decreased from 0.085 ($\pm$0.016) min^{-1} to 0.044 ($\pm$0.0077) min^{-1} when phosphate concentration increased from 0 to 1 mM (Figure 3.5). A similar trend was observed when the ionic strength was maintained at 10 mM. The deposition rate coefficient decreased from 0.058 ($\pm$0.012) min^{-1} to

0.0060 ($\pm$0.00064) min^{-1} when phosphate concentration increased from 0 to 1 mM, respectively.

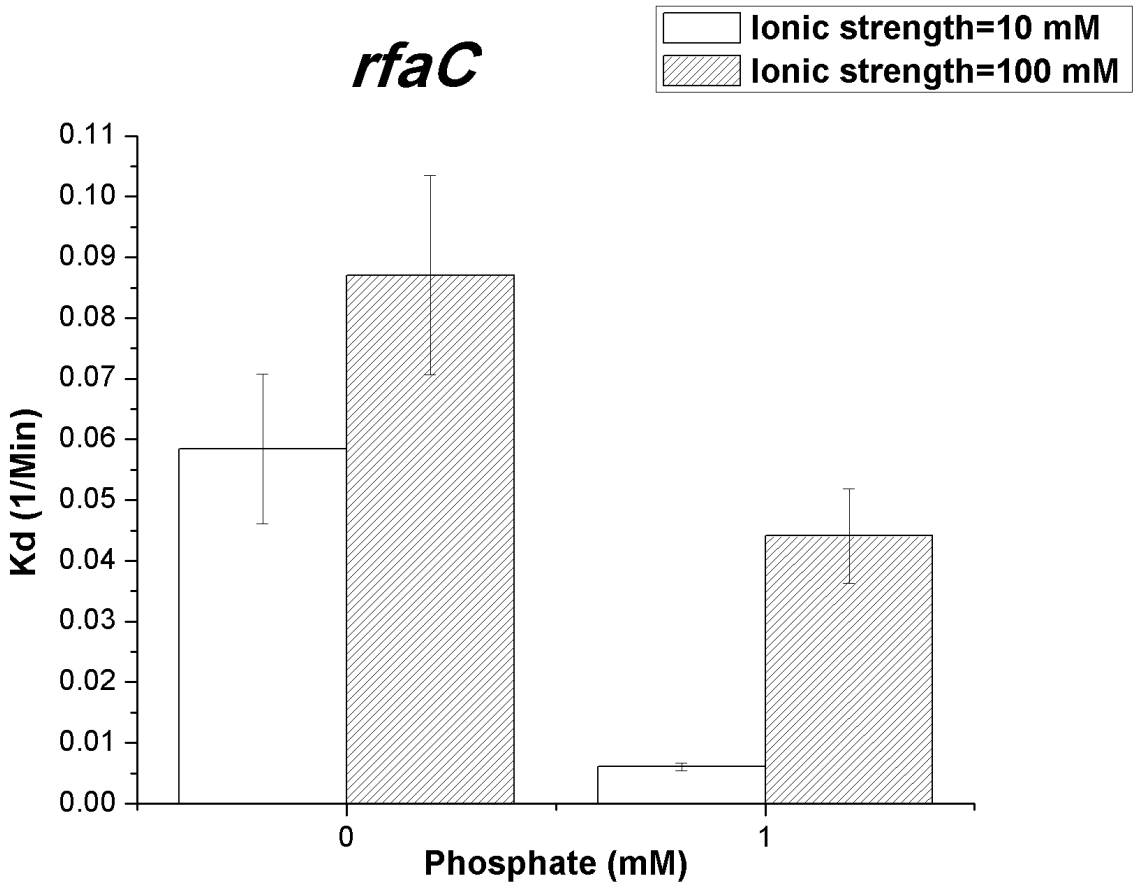

Figure 3.5 Bacteria's deposition rate coefficient (kd) of rfaC cells was determined from the breakthrough curves using Equation 2.1 under both ionic strengths. Experimental conditions were: approach velocity = 0.31 cm/min, porosity = 0.344 and pH = 7.2. Error bars represent standard deviations of triplicate measurements.

Figure 3.6 presents the comparison of deposition rate coefficient between *E.coli* O157:H7, *rfaC*, and *waaL* cells. The retention of *rfaC* cells within quartz sand was higher

than *waaL* under each condition. Consistent with findings reported in breakthrough curves.

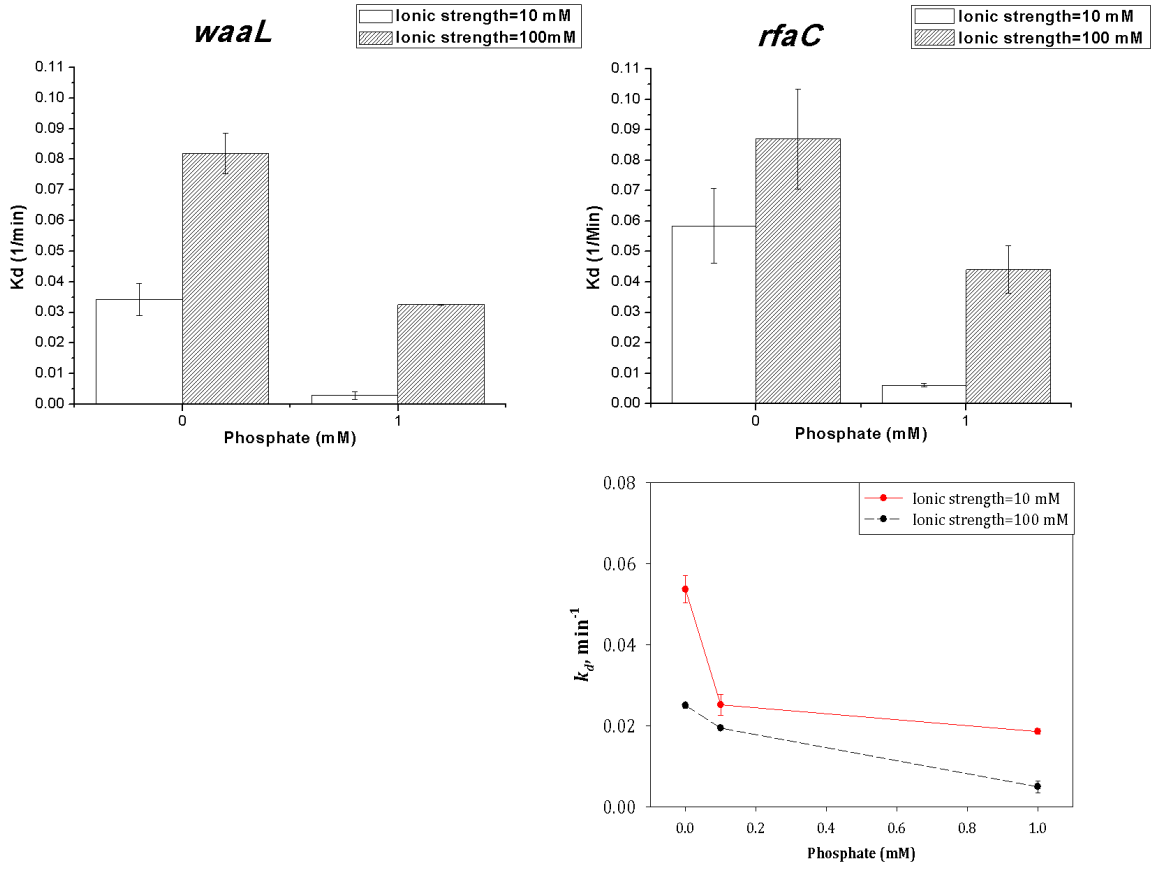

Figure 3.6 Comparison of deposition rate coefficient between E.coli O157:H7, rfaC, and waaL cells. Experimental conditions were: approach velocity = 0.31 cm/min, porosity = 0.344 and pH = 7.2. Error bars represent standard deviations of triplicate measurements.

3.3. Zeta Potential of *E.coli* O157:H7, *rfaC*, and *waaL* Cells

Figure 3.7 represents zeta potentials of both *waaL* cells and quartz sand, which were negative. In general, the zeta potentials of sand were ~40 mV less negative when ionic strength increased from 10 mM to 100 mM due to the compression of electric double

layer. The zeta potentials of the *waaL* cells ~10 mV and ~30 mV less negative when ionic strengths are 100 mM and 10 mM. For both quartz sand and bacterial cells, an increase in ionic strength led to a decrease in the zeta potential of the bacterial cells (Figure 3.7). For both quartz sand and bacterial cells, phosphate decreased zeta potential values. This could be related to adsorption of phosphate onto the surface of quartz sand (e.g., through the bonding between phosphate phosphorus and oxygen at the surface of quartz) and bacterial cells, which could increase the negative surface charge under the pH conditions employed in this research [112].

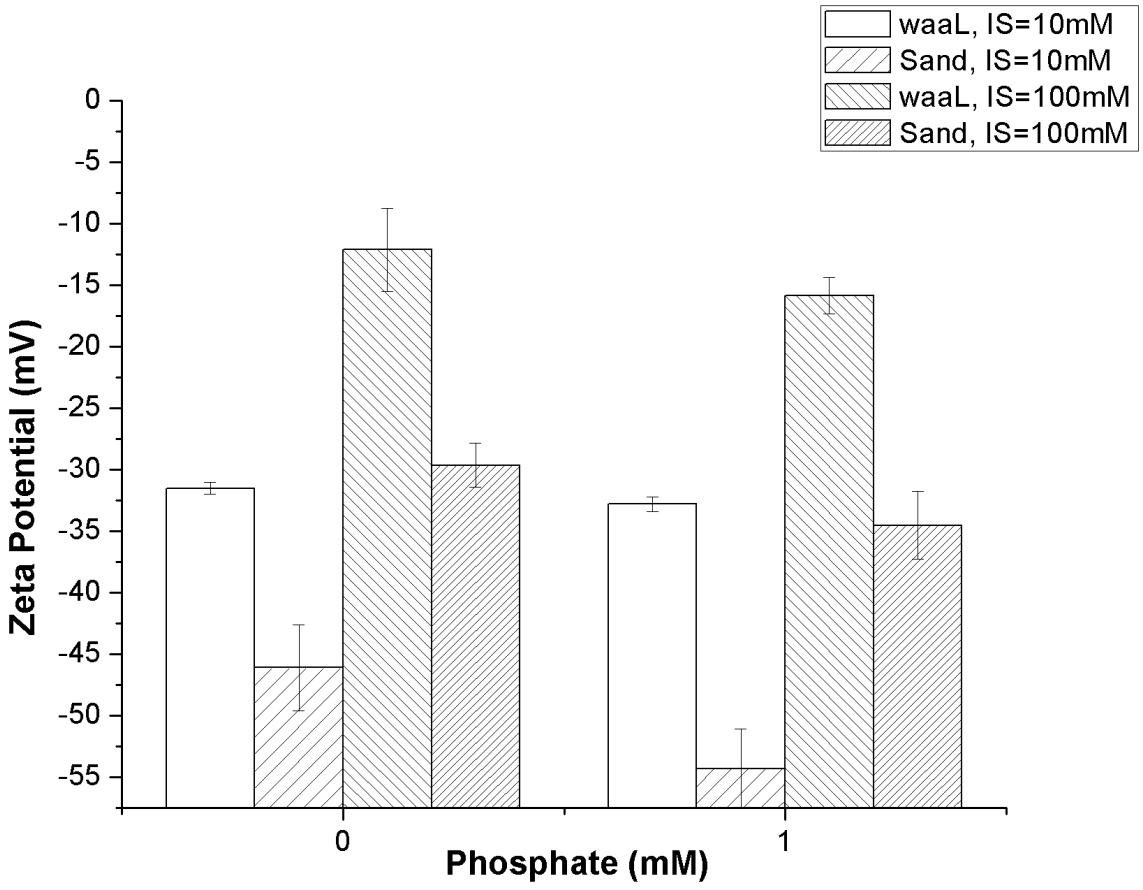

Figure 3.7 Surface zeta potential of waaL bacteria (core mutant) and saturated quartz sand, under two solution ionic strengths: 10 mM and 100 mM, as a function of solution

chemistry. Concentrations of phosphate were 0 and 1 mM. Error bars represent standard deviations of ten replicate measurements.

Figure 3.8 represents zeta potentials of both *rfaC* cells and quartz sand, which were negative. In general, the zeta potentials of sand were ∼35 mV less negative when ionic strength increased from 10 mM to 100 mM due to the compression of electric double layer. The zeta potentials of the *rfaC* cells ∼10 mV and ∼30 mV less negative when ionic strengths are 100 mM and 10 mM. For both quartz sand and bacterial cells, an increase in ionic strength led to a decrease in the zeta potential of the bacterial cells (Figure 3.8). For both quartz sand and bacterial cells, phosphate decreased zeta potential values. This could be related to adsorption of phosphate onto the surface of quartz sand (e.g., through the bonding between phosphate phosphorus and oxygen at the surface of quartz) and bacterial cells, which could increase the negative surface charge under the pH conditions employed in this research [112].

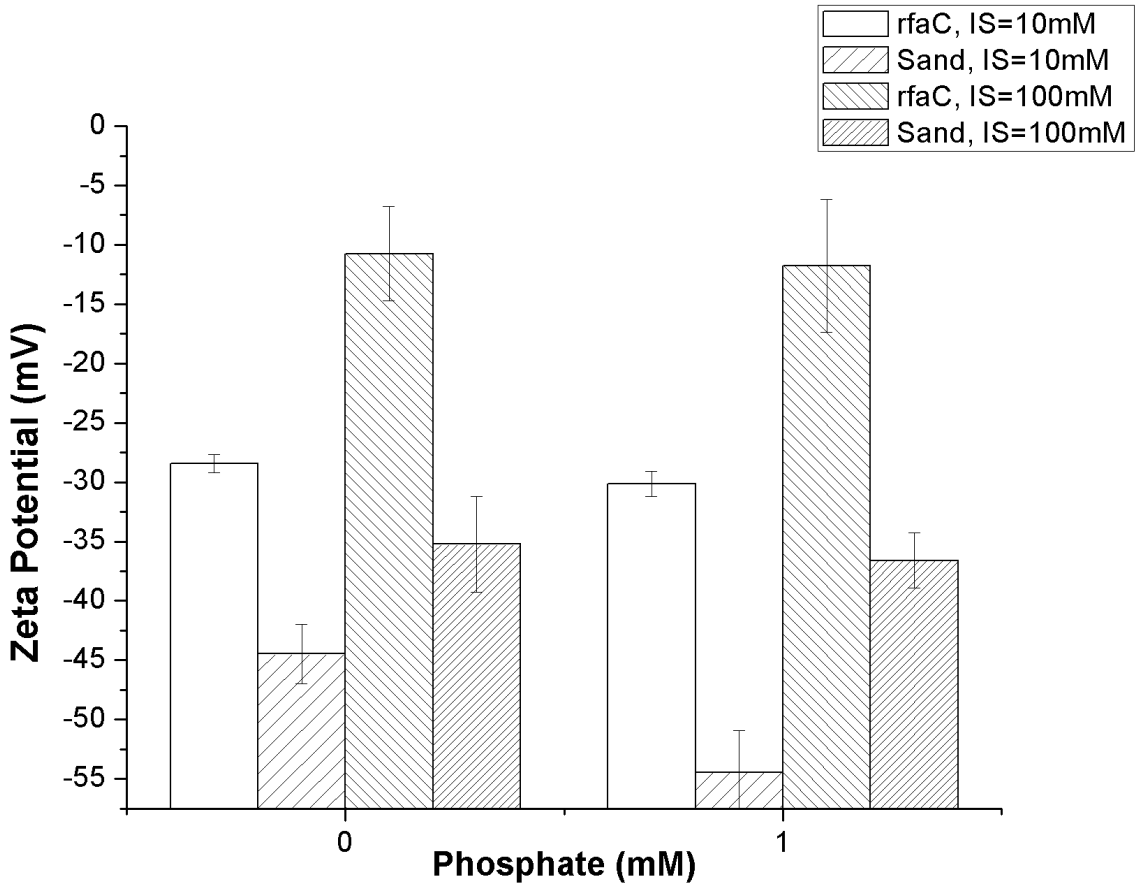

Figure 3.8 Surface zeta potential of rfaC bacteria (O-antigen mutant) and saturated quartz sand, under two solution ionic strengths: 10 mM and 100 mM, as a function of solution chemistry. Concentrations of phosphate were 0 and 1 mM. Error bars represent standard deviations of ten replicate measurements.

Figure 3.9 presents the comparison of zeta potential between *E.coli* O157:H7, *rfaC*, and *waaL* cells.

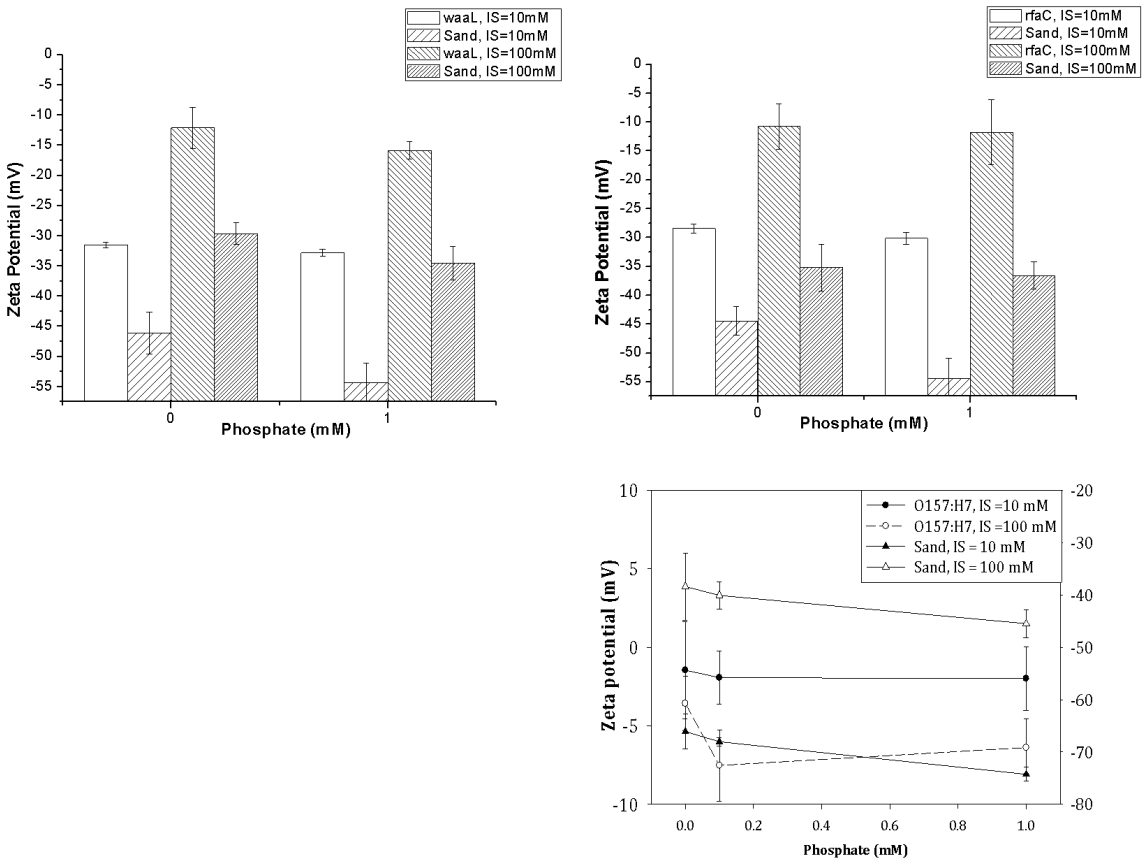

Figure 3.9 Comparison of zetapotential between E.coli O157:H7, rfaC, and waaL cells. Error bars represent standard deviations of ten replicate measurements.

3.4. Steric Energy Interaction of *E.coli* O157:H7, *rfaC*, and *waaL* Cells

Figure 3.10 indicates that the steric interaction between *rfaC* surface and quartz sand was significantly higher than the XDLVO forces at comparable distances. This is qualitatively consistent with our observation that retention of *rfaC* is reversible when the XDLVO theory predicts the absence of energy barrier. Additionally, it has been hypothesized that the conformational changes caused by the deprotonation of bacterial surface lipopolysaccharides carboxylic and phosphoric functional groups allowed for

greater penetration of the counterions into the polymer layer, which in turn decreased the attachment of *rfaC* cells onto the surface of quartz sand.

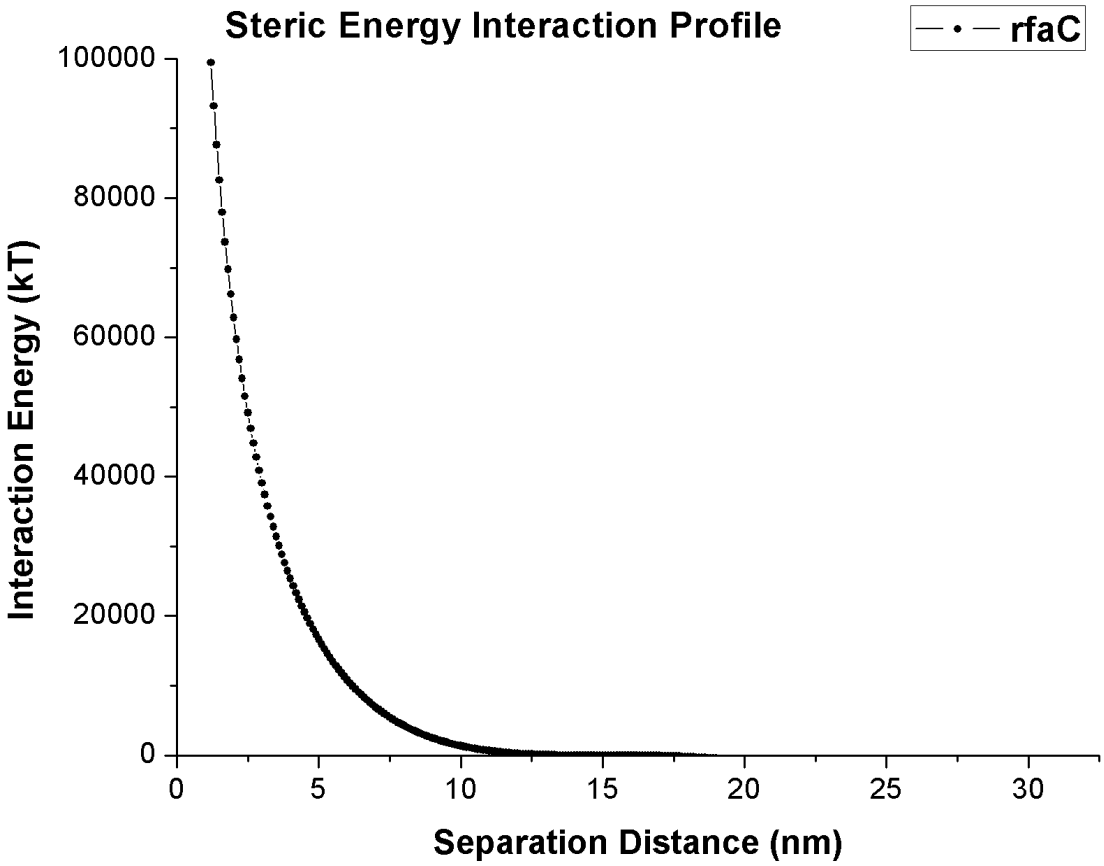

Figure 3.10 Steric interaction energy profile between rfaC cells and surface of quartz sands. The energy interaction was expressed in kT, where k is Boltzmann constant and T is absolute temperature in Kelvin.

Figure 3.11 indicates that the steric interaction between *waaL* surface and quartz sand was significantly higher than the XDLVO forces at comparable distances. This is qualitatively consistent with our observation that retention of *waaL* is reversible when the XDLVO theory predicts the absence of energy barrier. Additionally, it has been

hypothesized that the conformational changes caused by the deprotonation of bacterial surface lipopolysaccharides carboxylic and phosphoric functional groups allowed for greater penetration of the counterions into the polymer layer, which in turn decreased the attachment of *waaL* cells onto the surface of quartz sand.

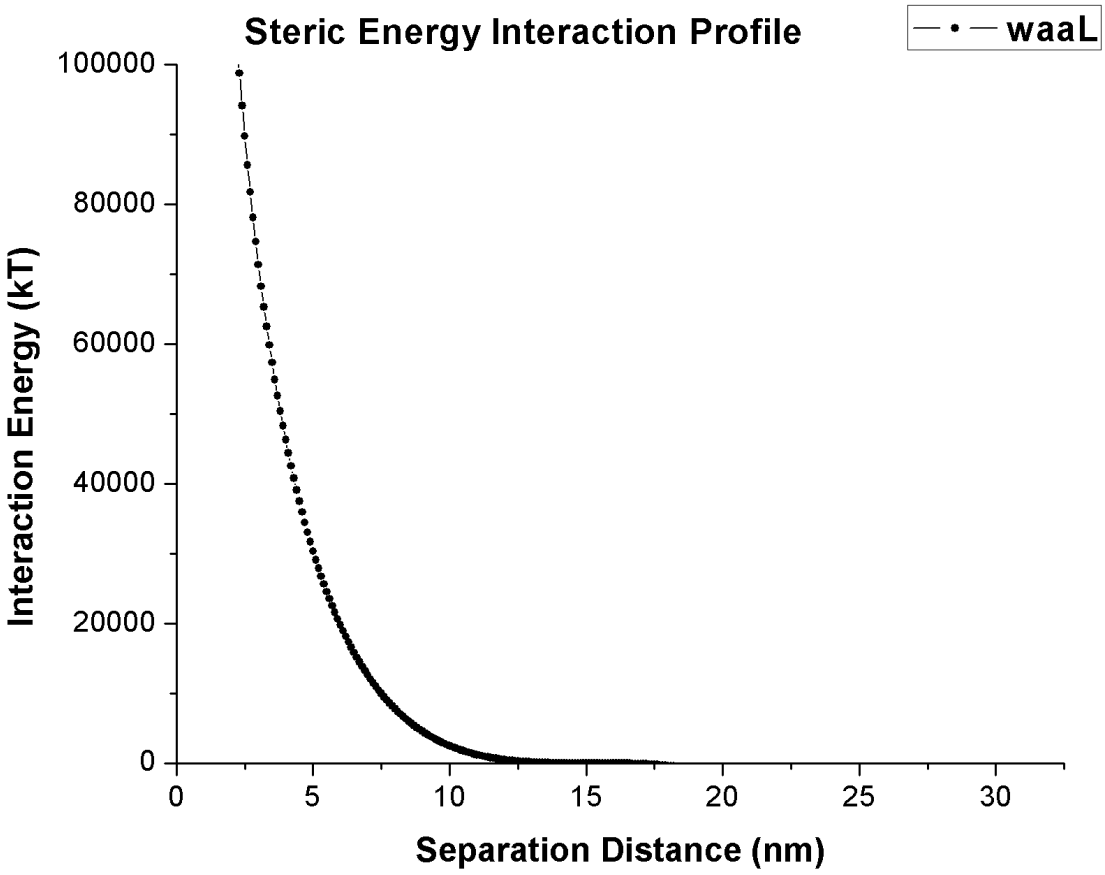

Figure 3.11 Steric interaction energy profile between waaL cells and surface of quartz sands. The energy interaction was expressed in kT, where k is Boltzmann constant and T is absolute temperature in Kelvin.

Figure 3.12 presents the comparison of steric energy interaction profile between *E.coli* O157:H7, *rfaC*, and *waaL* cells.

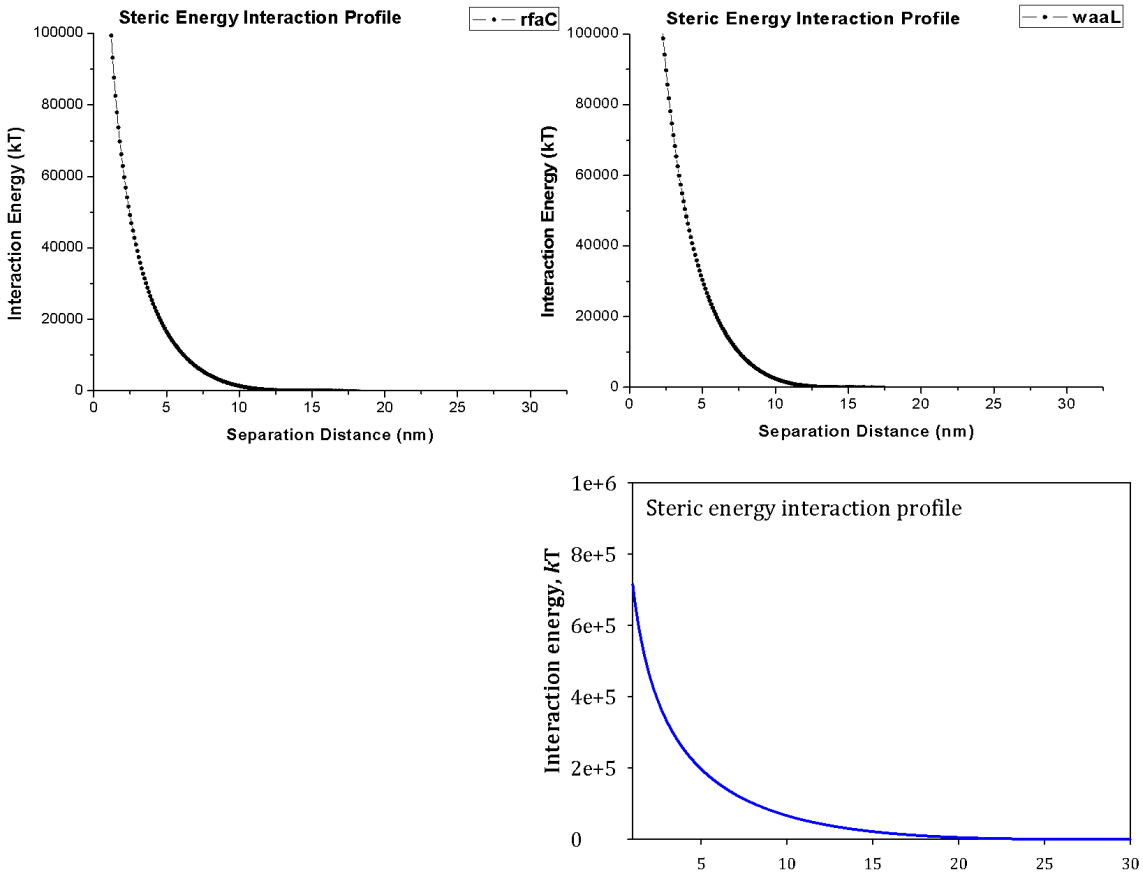

Figure 3.12 presents the comparison of steric energy interaction profile between E.coli O157:H7, rfaC, and waaL cells.

3.5. XDLVO Interaction Energy Profiles

The measured contact angles of water, glycerol, and diiodomethane on *waaL* bacteria were 47° (±0.2°), 32.3° (±1.1°) and 54.8° (±0.6°), respectively. The values of γ^{LW}, γ^{-} and γ^{+} for *waaL* bacteria are calculated as 31.6, 21.9 and 5.0 mJm^{-2}, respectively. Using the values previously determined for quartz in Morrow et al.,[107] the Hamaker constant in Equation 2.4 for the bacterium-water-quartz system was estimated as

2.81×10^{-21} J. The estimated value of $\Delta G_{h_0}^{AB}$ in Equation 2.7 was 7.6 mJm^{-2}, suggesting a repulsive AB interaction between the *waaL* cells and the quartz sand.

Figure 3.13 presents the calculated XDLVO energy interaction profiles of *waaL* bacteria. Energy barrier were present when phosphate concentrations were 0 mM and 1 mM under both ionic strengths which were 10 mM and 100 mM. At the ionic strength of 100 mM, the first energy barrier (Figure 3.10 A) values were 84.1kT (No phosphate) and 217 kT (1 mM phosphate), respectively, where k is the Boltzmann constant and T is the absolute temperature in Kelvin. The secondary energy minimum (Figure 3.10 B) values were 15.4 kT (No phosphate) and 14.7 kT (1 mM phosphate). Similarly, when ionic strength was 10 mM, the first energy barrier changed from 13800 kT to 15000 kT for both 0 mM and 1 mM phosphate. The secondary energy minimums were 3.4 kT (No phosphate) and 3 kT (1 mM phosphate).

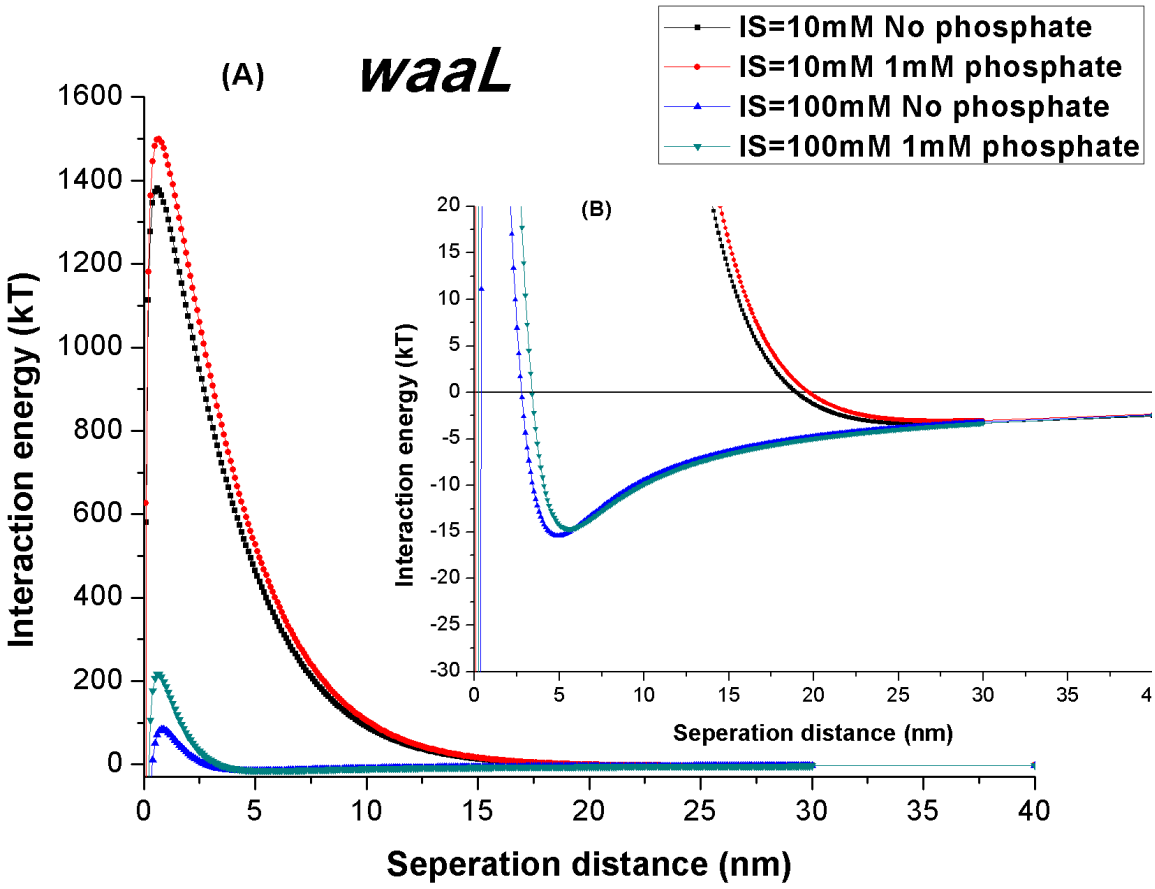

Figure 3.13 XDLVO interaction energy profiles of waaL bacteria in clean column with different phosphate concentrations under different ionic strengths. Insets highlight the locations of the secondary energy minima.

The measured contact angles of water, glycerol, and diiodomethane on *rfaC* bacteria were 28.1° (±0.4°), 25° (±0.9°) and 48.7° (±0.5°), respectively. The values of γ^{LW}, γ^{-} and γ^{+} for *rfaC* bacteria are calculated as 35, 38.7 and 3.5 mJm^{-2}, respectively. Using the values previously determined for quartz in Morrow et al.,[107] the Hamaker constant in Equation 2.4 for the bacterium-water-quartz system was estimated as 3.69×10^{-21} J. The estimated value of $\Delta G_{h_0}^{AB}$ in Equation 2.7 was 20.9 mJm^{-2}, suggesting a repulsive AB interaction between the *rfaC* cells and the quartz sand.

Figure 3.14 presents the calculated XDLVO energy interaction profiles of *rfaC* bacteria. Energy barrier were present when phosphate concentrations were 0 mM and 1 mM under both ionic strengths which were 10 mM and 100 mM. At the ionic strength of 100 mM, the first energy barrier (Figure 3.11 A) values were 46.7kT (No phosphate) and 76.6 kT (1 mM phosphate), respectively, where k is the Boltzmann constant and T is the absolute temperature in Kelvin. The secondary energy minimum (Figure 3.11 B) values were 21.7 kT (No phosphate) and 21.4 kT (1 mM phosphate). Similarly, when ionic strength was 10 mM, the first energy barrier changed from 11000 kT to 12600 kT for both 0 mM and 1 mM phosphate. The secondary energy minimums were 4.73 kT (No phosphate) and 4.2 kT (1 mM phosphate).

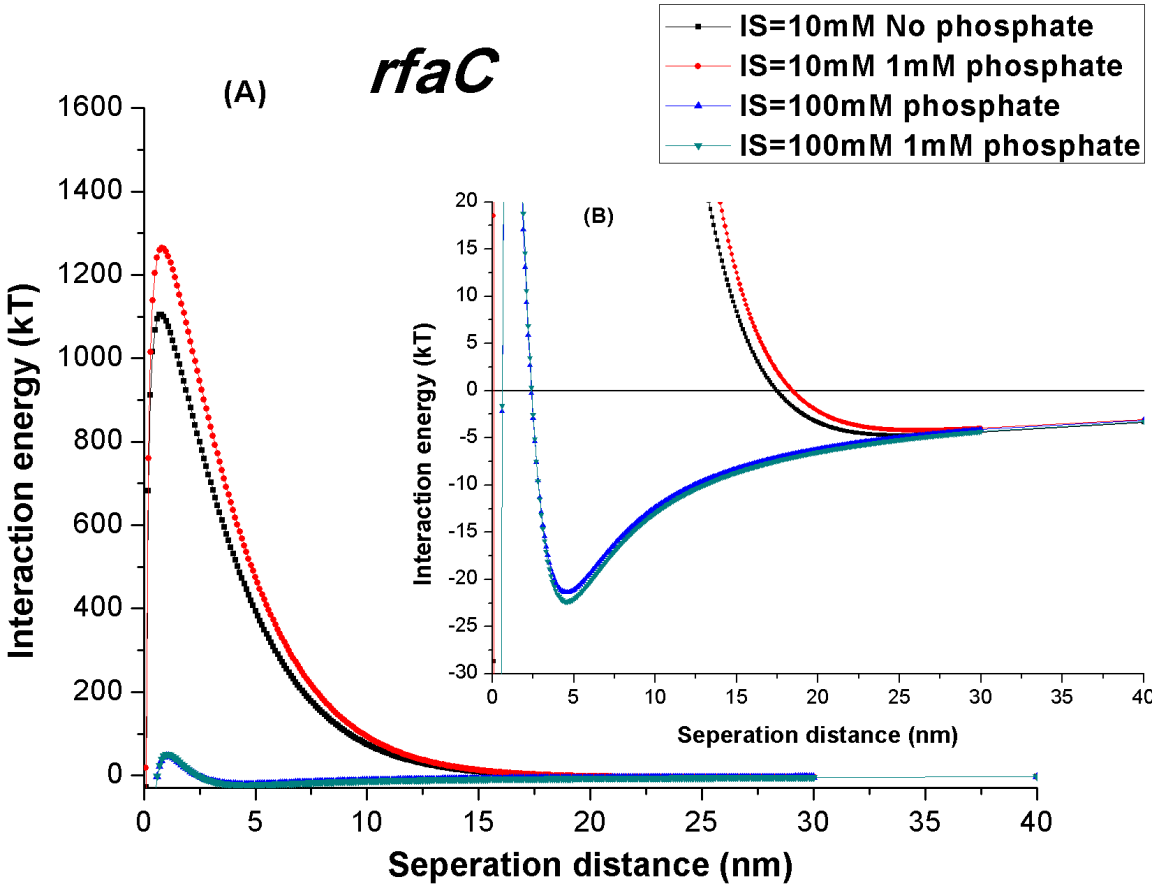

Figure 3.14 XDLVO interaction energy profiles of rfaC bacteria in clean column with different phosphate concentrations under different ionic strengths. Insets highlight the locations of the secondary energy minima.

Figure 3.15 presents the comparison of interactional energy profiles of *E.coli* O157:H7, *rfaC*, and *waaL* cells. The interaction energy of *waaL* was higher than *rfaC* in the primary energy barrier. In the secondary energy minimum, *rfaC* went deeper than *waaL*. Majority deposition of *rfaC* cells happened in the secondary energy minima.

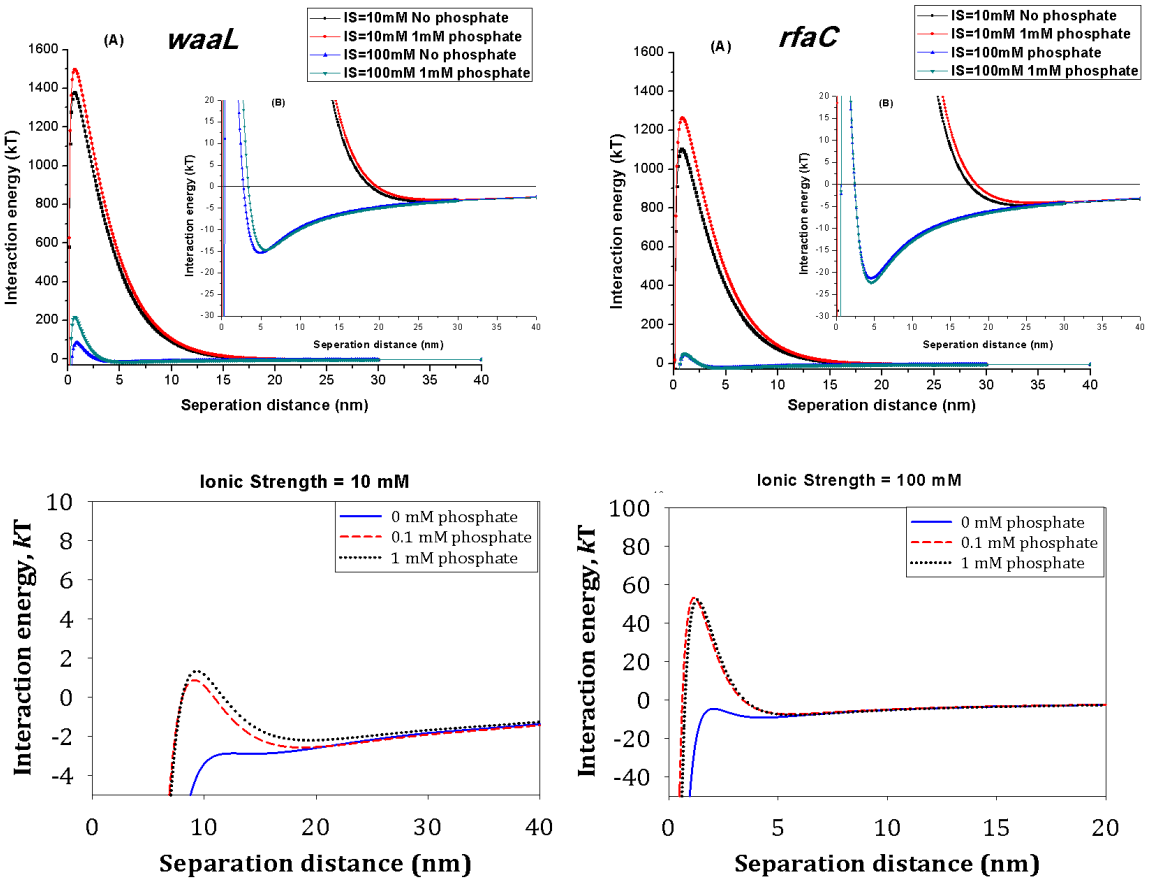

Figure 3.15 Comparison of interactional energy profiles of E.coli O157:H7, rfaC, and waaL cells. Experimental conditions were: approach velocity = 0.31 cm/min, porosity = 0.344 and pH = 7.2. Error bars represent standard deviations of triplicate measurements.

4. Discussion

4.1. Transport of *E. coli* O157:H7, *rfaC* and *waaL* cells within Sand Packs.

It was reported that under high pH (>8.4) conditions, the retention of *E. coli* O157:H7 cells within quartz sand increased with decreasing ionic strength [113]. Consistent with findings in previous research, results from our study show that the deposition of *E. coli*

O157:H7, *rfaC* and *waaL* cells increased with decreasing ionic strength under a pH of 7.2, regardless of phosphate concentrations (Figures 3.3 and 3.6). For instance, in the absence of phosphate, the deposition rate coefficients of *rfaC* were 0.082 ($\pm$0.0066) min^{-1} and 0.034 ($\pm$0.0052) min^{-1} for 10 and 100 mM of ionic strength, respectively. A similar trend in deposition rate coefficients of *waaL*, results were 0.085 ($\pm$0.016) min^{-1} and 0.058 ($\pm$0.012) min^{-1} for 10 and 100 mM of ionic strength solutions, respectively.

The zeta potentials of *E. coli* O157:H7, *rfaC* and *waaL* cells were less negative, and in contrast to the trend observed for quartz sand, an increase in ionic strength led to a slight decrease in the zeta potential of the bacterial cells (Figure 3.9). For both quartz sand and bacteria cells, phosphate decreased zeta potential values. This could be related to adsorption of phosphate onto the surface of quartz sand (e.g., through the bonding between phosphorus and oxygen at the surface of quartz) and bacterial cells, which could increase the negative surface charge under the pH conditions employed in this research [112].

The energy barriers (Figure 3.12), could indicate the attachment of *E. coli* O157:H7, *rfaC* and *waaL* cells to the surface of quartz sand and thus change a system that would make it unfavorable for deposition. This trend is consistent with results from the packed-bed column transport experiments, which suggest that phosphate increased the transport of *E. coli* O157:H7, *rfaC* and *waaL* cells. Additionally, the magnitude of the energy barriers was generally higher for the 100 mM ionic strength conditions than the 10 mM ionic strength conditions. This is consistent with the observation that the transport of *E. coli*

O157:H7, *rfaC* and *waaL* cells within the quartz sand columns increased with higher ionic strength (Figures 3.3 and 3.6).

Moreover, the magnitudes of the energy barriers of *rfaC* cells were higher than *waaL* cells under each conditions (Figure 3.12). This trend is consistent with the results from packed-bed columns experiment that the retention of *waaL* cells within quartz sand is higher than *rfaC* cells under each conditions (Figure 3.6).

The total XDLVO energy interaction profiles reflect the summation of the LW, EDL, and AB interactions. The LW and AB components of the overall interaction energy are independent of water chemistry parameters and remain the same for all conditions. Ionic strength, however, had a significant impact on the zeta potential of *E. coli* O157:H7, *rfaC* and *waaL* cells and the sands (Figure 3.9). As the sand zeta potential became less negative when ionic strength increased from 10 to 100 mM, the zeta potential of *E. coli* O157:H7, *rfaC* and *waaL* cells became more negative. In response to the changes in the zeta potential values, the calculated EDL interactions between bacterial cells and quartz sand under 100 mM ionic strength conditions were more repulsive than the EDL interactions under 10 mM ionic strength conditions.

4.2. Role of Secondary Energy Minimum on the transport of *E. coli* O157:H7, *rfaC* and *waaL* cells.

It was reported that bacterial deposition is likely occurring in the secondary energy minimum, which DLVO calculations indicated increases in depth with ionic strength [57].

The van der Waals and electrostatic double layer interactions have different dependencies with respect to separation distance. Therefore, calculations of the total interaction energy profiles predict the presence of a secondary energy minimum at a greater separation distance than that of the energy barrier (Figure 3.12). The XDLVO profiles are highlighted in Figure 3.10 and 3.11 to indicate the magnitude of this secondary energy minimum.

Bacteria approaching quartz sand would first experience an attractive force before encountering the significant repulsive energy barrier. Cells unable to overcome the energy barrier could remain associated with the quartz sand within the secondary energy minimum unless they had sufficient energy to escape. The magnitude of the secondary energy minimum increases with ionic strength. For instance, the depth of secondary minima of *rfaC* cells ranges from 3.4 kT at 10 mM to 15.4 kT at 100 mM, with corresponding separation distances of 4 to 24 nm and the absent of phosphate, respectively.

The secondary minimum depths discussed previously were calculated by assuming that electrostatic component of the XDLVO interactions followed the Hogg et al. expression for interaction at constant surface potentials [114]. Other models for calculating electrostatic interactions include assuming a constant surface charge or by compromising between the two approaches and relaxing the assumption of constant charge or potential, the so-called linear superposition approximation (LSA) [65]. The three models of electrostatic interactions are similar for separation distances greater

than about 5 nm; however, at closer distances they show significant different behavior. Therefore, predictions of the presence or absence on an energy barrier and a secondary energy minimum at moderate to high ionic strengths are strongly dependent on the model chosen for the calculation of electrostatic double layer interaction.

REFERENCES

1. McCarthy, J.F. and L.D. McKay, *Colloid transport in the subsurface: Past, present, and future challenges.* Vadose Zone Journal, 2004. **3**(2): p. 326-337.

2. Li, J., S. McLellan, and S. Ogawa, *Accumulation and fate of green fluorescent labeled Escherichia coli in laboratory-scale drinking water biofilters.* Water Research, 2006. **40**(16): p. 3023-3028.

3. Abu-Lail, N.I. and T.A. Camesano, *Role of lipopolysaccharides in the adhesion, retention, and transport of Escherichia coli JM109.* Environmental Science & Technology, 2003. **37**(10): p. 2173-2183.

4. Bradford, S.A. and M. Bettahar, *Straining, attachment, and detachment of Cryptosporidium oocysts in saturated porous media.* Journal of Environmental Quality, 2005. **34**(2): p. 469-478.

5. Walker, S.L.R., J.A, *influence of growth phase on bacterial deposition: interaction mechanisms in packed-bed column and radial stagnation point flow system.* Environ. Sci. Technol, 2005. **39(17), 6405-6411**.

6. Liu, Y.Y., C-H.; Li, J, *Influence of extracellular polymeric substances on Pseudomonas aeruginosa transport and deposition profiles in porous media.* Environ. Sci. Technol., 2007. **41(1), 198-205**.

7. Camper, A.K., et al., *Effects of Motility and Adsorption Rate Coefficient on Transport of Bacteria through Saturated Porous-Media.* Applied and Environmental Microbiology, 1993. **59**(10): p. 3455-3462.

8. Camesano, T.A. and B.E. Logan, *Influence of fluid velocity and cell concentration on the transport of motile and nonmotile bacteria in porous media.* Environmental Science & Technology, 1998. **32**(11): p. 1699-1708.

9. Tufenkji, N., J.A. Redman, and M. Elimelech, *Interpreting deposition patterns of microbial particles in laboratory-scale column experiments.* Environmental Science & Technology, 2003. **37**(3): p. 616-623.

10. Bradford, S.A., et al., *Physical factors affecting the transport and fate of colloids in saturated porous media.* Water Resources Research, 2002. **38**(12).

11. Simoni, S.F., et al., *Population heterogeneity affects transport of bacteria through sand columns at low flow rates.* Environmental Science & Technology, 1998. **32**(14): p. 2100-2105.

12. Jucker, B.A., et al., *Adsorption of bacterial surface polysaccharides on mineral oxides is mediated by hydrogen bonds.* Colloids and Surfaces B-Biointerfaces, 1997. **9**(6): p. 331-343.

13. Jucker, B.A., H. Harms, and A.J.B. Zehnder, *Polymer interactions between five gram-negative bacteria and glass investigated using LPS micelles and vesicles as model systems.* Colloids and Surfaces B-Biointerfaces, 1998. **11**(1-2): p. 33-45.

14. Tsuneda, S., et al., *Extracellular polymeric substances responsible for bacterial adhesion onto solid surface.* Fems Microbiology Letters, 2003. **223**(2): p. 287-292.

15. Strauss, J.B., N.; Camesano, T., *atomic force microscopy study of the role of LPS O-antigen on adhesion of ecoli.* J. Mol. Recognit., 2009. **22, 347-355**.

16. Tsuneda, S., et al., *Influence of extracellular polymers on electrokinetic properties of heterotrophic bacterial cells examined by soft particle electrophoresis theory.* Colloids and Surfaces B-Biointerfaces, 2003. **29**(2-3): p. 181-188.

17. Jucker, B.A., A.J.B. Zehnder, and H. Harms, *Quantification of polymer interactions in bacterial adhesion.* Environmental Science & Technology, 1998. **32**(19): p. 2909-2915.

18. Chen, L. and W.G. Coleman, *CLONING AND CHARACTERIZATION OF THE ESCHERICHIA-COLI K-12 RFA-2 (RFAC) GENE, A GENE REQUIRED FOR LIPOPOLYSACCHARIDE INNER CORE SYNTHESIS.* Journal of Bacteriology, 1993. **175**(9): p. 2534-2540.

19. Klena, J.D., E. Pradel, and C.A. Schnaitman, *COMPARISON OF LIPOPOLYSACCHARIDE BIOSYNTHESIS GENES RFAK, RFAL, RFAY, AND RFAZ OF ESCHERICHIA-COLI K-12 AND SALMONELLA-TYPHIMURIUM.* Journal of Bacteriology, 1992. **174**(14): p. 4746-4752.

20. Walker, S.L., J.A. Redman, and M. Elimelech, *Role of cell surface lipopolysaccharides in Escherichia coli K12 adhesion and transport.* Langmuir, 2004. **20**(18): p. 7736-7746.

21. Liu, X.Y., G.X. Chen, and C.M. Su, *Influence of Collector Surface Composition and Water Chemistry on the Deposition of Cerium Dioxide Nanoparticles: QCM-D and Column Experiment Approaches.* Environmental Science & Technology, 2012. **46**(12): p. 6681-6688.

22. Haznedaroglu, B.Z., et al., *Relative Transport Behavior of Escherichia coli O157:H7 and Salmonella enterica Serovar Pullorum in Packed Bed Column Systems: Influence of Solution Chemistry and Cell Concentration.* Environmental Science & Technology, 2009. **43**(6): p. 1838-1844.

23. Rangel, J.M., et al., *Epidemiology of Escherichia coli O157 : H7 outbreaks, United States, 1982-2002.* Emerging Infectious Diseases, 2005. **11**(4): p. 603-609.

24. Garber, L.P., et al., *RISK-FACTORS FOR FECAL SHEDDING OF ESCHERICHIA-COLI O157-H7 IN DAIRY CALVES.* Journal of the American Veterinary Medical Association, 1995. **207**(1): p. 46-49.

25. Montenegro, M.A., et al., *DETECTION AND CHARACTERIZATION OF FECAL VEROTOXIN-PRODUCING ESCHERICHIA-COLI FROM HEALTHY CATTLE.* Journal of Clinical Microbiology, 1990. **28**(6): p. 1417-1421.

26. Zhao, T., et al., *PREVALENCE OF ENTEROHEMORRHAGIC ESCHERICHIA-COLI O157-H7 IN A SURVEY OF DAIRY HERDS.* Applied and Environmental Microbiology, 1995. **61**(4): p. 1290-1293.

27. Keene, W.E., et al., *A SWIMMING-ASSOCIATED OUTBREAK OF HEMORRHAGIC COLITIS CAUSED BY ESCHERICHIA-COLI O157-H7 AND SHIGELLA-SONNEI.* New England Journal of Medicine, 1994. **331**(9): p. 579-584.

28. Hancock, D.D., et al., *THE PREVALENCE OF ESCHERICHIA-COLI O157.H7 IN DAIRY AND BEEF-CATTLE IN WASHINGTON-STATE.* Epidemiology and Infection, 1994. **113**(2): p. 199-207.

29. Kotra, L.P., et al., *Dynamics of the lipopolysaccharide assembly on the surface of Escherichia coli.* Journal of the American Chemical Society, 1999. **121**(38): p. 8707-8711.

30. K.C.Marshall, *Mechanism of the Initial Events in the Sorption of Marine Bacteria to Surfaces.* Journal of General Microbiology, 1971.

31. Loosdrecht, M.C.M.v., *Electrophoretic Mobility and Hydrophobicity as a Measure To Predict the Initial Steps of Bacterial Adhesion.* Applied and Environmental Microbiology, 1987.

32. Loosdrecht, M.C.M.v., *The Role of Bacterial Cell Wall Hydrophobicity in Adhesion.* Applied and Environmental Microbiology, 1987.

33. Rijnaarts, H.H.M., et al., *THE ISOELECTRIC POINT OF BACTERIA AS AN INDICATOR FOR THE PRESENCE OF CELL-SURFACE POLYMERS THAT INHIBIT ADHESION.* Colloids and Surfaces B-Biointerfaces, 1995. **4**(4): p. 191-197.

34. Bostrom, M., D.R.M. Williams, and B.W. Ninham, *Specific ion effects: Why DLVO theory fails for biology and colloid systems.* Physical Review Letters, 2001. **87**(16).

35. Williams, V. and M. Fletcher, *Pseudomonas fluorescens adhesion and transport through porous media are affected by lipopolysaccharide composition.* Applied and Environmental Microbiology, 1996. **62**(1): p. 100-104.

36. Dufrene, Y.F. and G.U. Lee, *Advances in the characterization of supported lipid films with the atomic force microscope.* Biochimica Et Biophysica Acta-Biomembranes, 2000. **1509**(1-2): p. 14-41.

37. Dufrene, Y.F., *Application of atomic force microscopy to microbial surfaces: from reconstituted cell surface layers to living cells.* Micron, 2001. **32**(2): p. 153-165.

38. Dufrene, Y.F., et al., *Probing molecular interactions and mechanical properties of microbial cell surfaces by atomic force microscopy.* Ultramicroscopy, 2001. **86**(1-2): p. 113-120.

39. van der Aa, B.C., et al., *Stretching cell surface macromolecules by atomic force microscopy.* Langmuir, 2001. **17**(11): p. 3116-3119.

40. Boonaert, C.J.P., P.G. Rouxhet, and Y.F. Dufrene, *Surface properties of microbial cells probed at the nanometre scale with atomic force microscopy.* Surface and Interface Analysis, 2000. **30**(1): p. 32-35.

41. Camesano, T.A. and N.I. Abu-Lail, *Heterogeneity in bacterial surface polysaccharides, probed on a single-molecule basis.* Biomacromolecules, 2002. **3**(4): p. 661-667.

42. Abu-Lail, N.I. and T.A. Camesano, *Elasticity of Pseudomonas putida KT2442 surface polymers probed with single-molecule force microscopy.* Langmuir, 2002. **18**(10): p. 4071-4081.

43. Ong, Y.L., et al., *Adhesion forces between E-coli bacteria and biomaterial surfaces.* Langmuir, 1999. **15**(8): p. 2719-2725.

44. Wang, L.X., S.P. Xu, and J. Li, *Effects of Phosphate on the Transport of Escherichia coli O157:H7 in Saturated Quartz Sand.* Environmental Science & Technology, 2011. **45**(22): p. 9566-9573.

45. Appenzeller, B.M.R., et al., *Influence of phosphate on bacterial adhesion onto iron oxyhydroxide in drinking water.* Environmental Science & Technology, 2002. **36**(4): p. 646-652.

46. Park, S.J., C.G. Lee, and S.B. Kim, *The role of phosphate in bacterial interaction with iron-coated surfaces.* Colloids and Surfaces B-Biointerfaces, 2009. **68**(1): p. 79-82.

47. Miettinen, I.T., T. Vartiainen, and P.J. Martikainen, *Phosphorus and bacterial growth in drinking water.* Applied and Environmental Microbiology, 1997. **63**(8): p. 3242-3245.

48. Sathasivan, A., et al., *Role of inorganic phosphorus in controlling regrowth in water distribution system.* Water Science and Technology, 1997. **35**(8): p. 37-44.

49. Appenzeller, B.M.R., et al., *Effect of adding phosphate to drinking water on bacterial growth in slightly and highly corroded pipes.* Water Research, 2001. **35**(4): p. 1100-1105.

50. Lechevallier, M.W., et al., *EXAMINING THE RELATIONSHIP BETWEEN IRON CORROSION AND THE DISINFECTION OF BIOFILM BACTERIA.* Journal American Water Works Association, 1993. **85**(7): p. 111-123.

51. Geelhoed, J.S., T. Hiemstra, and W.H. Van Riemsdijk, *Competitive interaction between phosphate and citrate on goethite.* Environmental Science & Technology, 1998. **32**(14): p. 2119-2123.

52. Bayoudh, S., et al., *Assessing bacterial adhesion using DLVO and XDLVO theories and the jet impingement technique.* Colloids and Surfaces B-Biointerfaces, 2009. **73**(1): p. 1-9.

53. Farahat, M., et al., *Adhesion of Escherichia coli onto quartz, hematite and corundum: Extended DLVO theory and flotation behavior.* Colloids and Surfaces B-Biointerfaces, 2009. **74**(1): p. 140-149.

54. Derjaguin, B.V.L., L.D., *Acta Physicochim.* U.S.S.R., 1941. **14,300**.

55. Verwey, E.J.W.O., J. T. G., *Theory of the Stability of Lyophobic Colloids: The Interaction of Sol Particles Having an Electric Double Layer.* Elsevier, 1948.

56. Walker, S.L., J.A. Redman, and M. Elimelech, *Influence of growth phase on bacterial deposition: Interaction mechanisms in packed-bed column and radial stagnation point flow systems.* Environmental Science & Technology, 2005. **39**(17): p. 6405-6411.

57. Redman, J.A., S.L. Walker, and M. Elimelech, *Bacterial adhesion and transport in porous media: Role of the secondary energy minimum.* Environmental Science & Technology, 2004. **38**(6): p. 1777-1785.

58. R.J., V.O.C.J.G., *Nature of the antigen-antibody interaction. Primary and secondary bonds: optimal conditions for association and dissociation.* J. Colloid Interface Sci., 1986. **376, 111-9**.

59. Brant, J.A. and A.E. Childress, *Membrane-colloid interactions: Comparison of extended DLVO predictions with AFM force measurements.* Environmental Engineering Science, 2002. **19**(6): p. 413-427.

60. Hwang, G., et al., *Determination of reliable Lewis acid-base surface tension components of a solid in LW-AB approach.* Journal of Industrial and Engineering Chemistry, 2011. **17**(1): p. 125-129.

61. Azeredo, J., J. Visser, and R. Oliveira, *Exopolymers in bacterial adhesion: interpretation in terms of DLVO and XDLVO theories.* Colloids and Surfaces B-Biointerfaces, 1999. **14**(1-4): p. 141-148.

62. Meinders, J.M., H.C. vanderMei, and H.J. Busscher, *Deposition efficiency and reversibility of bacterial adhesion under flow.* Journal of Colloid and Interface Science, 1995. **176**(2): p. 329-341.

63. Yao, K.M.H., M. T.; O'Melia, C. R., *Water and wastewater filtration: concepts and applications.* Environ. Sci. Technol., 1971. **5 (11), 1105-1112**.

64. Rajagopalan, R.T., C., *Trajectory analysis of deep-bed filtration with the sphere-in-cell porous media model.* AIChE J., 1976. **22 (3), 523-533**.

65. Elimelech, M.G., J.; Jia, X.; Williams, R. A., *Particle Deposition and Aggregation: Measurement, Modeling and simulation*1995, Woburn, MA: Butterworth-Heinemann.

66. Zobell, C.E., *The effect of solid surfaces on bacterial activity.* J Bacteriol, 1943. **46, 39-56**.

67. de Kerchove, A.J. and M. Elimelech, *Relevance of electrokinetic theory for "soft" particles to bacteria cells: Implications to bacterial adhesion.* Abstracts of Papers of the American Chemical Society, 2004. **228**: p. U633-U633.

68. Bradford, S.A., et al., *Straining of colloids at textural interfaces.* Water Resources Research, 2005. **41**(10).

69. Davey, M.E. and G.A. O'Toole, *Microbial biofilms: from ecology to molecular genetics.* Microbiology and Molecular Biology Reviews, 2000. **64**(4): p. 847-+.

70. deBeer, D. and P. Stoodley, *Relation between the structure of an aerobic biofilm and transport phenomena?* Water Science and Technology, 1995. **32**(8): p. 11-18.

71. Searcy, K.E., et al., *Capture and retention of Cryptosporidium parvum oocysts by Pseudomonas aeruginosa biofilms.* Applied and Environmental Microbiology, 2006. **72**(9): p. 6242-6247.

72. Oshea, S.J., M.E. Welland, and T. Rayment, *AN ATOMIC-FORCE MICROSCOPE STUDY OF GRAFTED POLYMERS ON MICA.* Langmuir, 1993. **9**(7): p. 1826-1835.

73. Iliuta, I. and F. Larachi, *Dynamics of cells attachment, aggregation, growth and detachment in trickle-bed bioreactors.* Chemical Engineering Science, 2006. **61**(15): p. 4893-4908.

74. Buswell, C.M., et al., *Extended survival and persistence of Campylobacter spp. in water and aquatic biofilms and their detection by immunofluorescent-antibody and -rRNA staining.* Applied and Environmental Microbiology, 1998. **64**(2): p. 733-741.

75. Grossart, H.P., et al., *Bacterial colonization of particles: Growth and interactions.* Applied and Environmental Microbiology, 2003. **69**(6): p. 3500-3509.

76. Camper, A.K., W.L. Jones, and J.T. Hayes, *Effect of growth conditions and substratum composition on the persistence of coliforms in mixed-population biofilms.* Applied and Environmental Microbiology, 1996. **62**(11): p. 4014-4018.

77. Langmark, J., et al., *Accumulation and fate of microorganisms and microspheres in biofilms formed in a pilot-scale water distribution system.* Applied and Environmental Microbiology, 2005. **71**(2): p. 706-712.

78. Williams, M.M. and E.B. Braun-Howland, *Growth of Escherichia coli in model distribution system biofilms exposed to hypochlorous acid or monochloramine.* Applied and Environmental Microbiology, 2003. **69**(9): p. 5463-5471.

79. Skvarla, J., *Does the hydrophobic attraction contribute to the interaction between colloidal silica spheres coagulated by an adsorbing cationic surfactant?* Colloids and Surfaces a-Physicochemical and Engineering Aspects, 2012. **397**: p. 33-41.

80. Rutland, M., A. Waltermo, and P. Claesson, *PH-DEPENDENT INTERACTIONS OF MICA SURFACES IN AQUEOUS DODECYLAMMONIUM DODECYLAMINE SOLUTIONS.* Langmuir, 1992. **8**(1): p. 176-183.

81. Parker, J.L., V.V. Yaminsky, and P.M. Claesson, *SURFACE FORCES BETWEEN GLASS SURFACES IN CETYLTRIMETHYLAMMONIUM BROMIDE SOLUTIONS.* Journal of Physical Chemistry, 1993. **97**(29): p. 7706-7710.

82. Parker, J.L., P.M. Claesson, and P. Attard, *BUBBLES, CAVITIES, AND THE LONG-RANGED ATTRACTION BETWEEN HYDROPHOBIC SURFACES.* Journal of Physical Chemistry, 1994. **98**(34): p. 8468-8480.

83. Parker, J.L. and P.M. Claesson, *FORCES BETWEEN HYDROPHOBIC SILANATED GLASS SURFACES.* Langmuir, 1994. **10**(3): p. 635-639.

84. Rabinovich, Y.I. and R.H. Yoon, *USE OF ATOMIC-FORCE MICROSCOPE FOR THE MEASUREMENTS OF HYDROPHOBIC FORCES.* Colloids and Surfaces a-Physicochemical and Engineering Aspects, 1994. **93**: p. 263-273.

85. Rabinovich, Y.I. and R.H. Yoon, *USE OF ATOMIC-FORCE MICROSCOPE FOR THE MEASUREMENTS OF HYDROPHOBIC FORCES BETWEEN SILANATED SILICA PLATE AND GLASS SPHERE.* Langmuir, 1994. **10**(6): p. 1903-1909.

86. Yoon, R.H., D.H. Flinn, and Y.I. Rabinovich, *Hydrophobic interactions between dissimilar surfaces.* Journal of Colloid and Interface Science, 1997. **185**(2): p. 363-370.

87. Yakubov, G.E., H.J. Butt, and O.I. Vinogradova, *Interaction forces between hydrophobic surfaces. Attractive jump as an indication of formation of "stable" submicrocavities.* Journal of Physical Chemistry B, 2000. **104**(15): p. 3407-3410.

88. Zhang, X.Y., Y.X. Zhu, and S. Granick, *Softened hydrophobic attraction between macroscopic surfaces in relative motion.* Journal of the American Chemical Society, 2001. **123**(27): p. 6736-6737.

89. Sakamoto, M., et al., *Origin of long-range attractive force between surfaces hydrophobized by surfactant adsorption.* Langmuir, 2002. **18**(15): p. 5713-5719.

90. Xu, Z.H. and R.H. Yoon, *THE ROLE OF HYDROPHOBIC INTERACTIONS IN COAGULATION.* Journal of Colloid and Interface Science, 1989. **132**(2): p. 532-541.

91. Zhou, Z.A., et al., *Effect of gas nuclei on the filtration of fine particles with different surface properties.* Colloids and Surfaces a-Physicochemical and Engineering Aspects, 1996. **113**(1-2): p. 67-77.

92. Gong, W.Q., et al., *The influence of dissolved gas on the interactions between surfaces of different hydrophobicity in aqueous media Part II. A spectroscopic study.* Physical Chemistry Chemical Physics, 1999. **1**(11): p. 2799-2803.

93. Zhou, Z.K., P.Q. Wu, and C.M. Ma, *HYDROPHOBIC INTERACTION AND STABILITY OF COLLOIDAL SILICA.* Colloids and Surfaces, 1990. **50**: p. 177-188.

94. Behrens, S.H., M. Borkovec, and P. Schurtenberger, *Aggregation in charge-stabilized colloidal suspensions revisited.* Langmuir, 1998. **14**(8): p. 1951-1954.

95. Behrens, S.H., et al., *Charging and aggregation properties of carboxyl latex particles: Experiments versus DLVO theory.* Langmuir, 2000. **16**(6): p. 2566-2575.

96. Kobayashi, M., et al., *Effects of heat treatment on the aggregation and charging of Stober-type silica.* Journal of Colloid and Interface Science, 2005. **292**(1): p. 139-147.

97. Kobayashi, M., et al., *Aggregation and charging of colloidal silica particles: Effect of particle size.* Langmuir, 2005. **21**(13): p. 5761-5769.

98. Walczak, J.J., et al., *Influence of tetracycline resistance on the transport of manure-derived Escherichia coil in saturated porous media.* Water Research, 2011. **45**(4): p. 1681-1690.

99. Brown, D.G. and P.R. Jaffe, *Effects of nonionic surfactants on bacterial transport through porous media.* Environmental Science & Technology, 2001. **35**(19): p. 3877-3883.

100. Kretzschmar, R., et al., *Experimental determination of colloid deposition rates and collision efficiencies in natural porous media.* Water Resources Research, 1997. **33**(5): p. 1129-1137.

101. Camesano, T.A. and B.E. Logan, *Probing bacterial electrosteric interactions using atomic force microscopy.* Environmental Science & Technology, 2000. **34**(16): p. 3354-3362.

102. Tong, M.P., et al., *Detachment-influenced transport of an adhesion-deficient bacterial strain within water-reactive porous media.* Environmental Science & Technology, 2005. **39**(8): p. 2500-2508.

103. Tong, M.P., T.A. Camesano, and W.P. Johnson, *Spatial variation in deposition rate coefficients of an adhesion-deficient bacterial strain in quartz sand.* Environmental Science & Technology, 2005. **39**(10): p. 3679-3687.

104. Bayoudh, S., et al., *Quantification of the adhesion free energy between bacteria and hydrophobic and hydrophilic substrata.* Materials Science & Engineering C-Biomimetic and Supramolecular Systems, 2006. **26**(2-3): p. 300-305.

105. Elimelech, M., *PARTICLE DEPOSITION ON IDEAL COLLECTORS FROM DILUTE FLOWING SUSPENSIONS - MATHEMATICAL FORMULATION, NUMERICAL-SOLUTION, AND SIMULATIONS.* Separations Technology, 1994. **4**(4): p. 186-212.

106. Huang, X.F., S. Bhattacharjee, and E.M.V. Hoek, *Is Surface Roughness a "Scapegoat" or a Primary Factor When Defining Particle-Substrate Interactions?* Langmuir, 2010. **26**(4): p. 2528-2537.

107. Morrow, J.B., et al., *Macro- and manoscale observations of adhesive behavior for several E-coli strains (O157 : H7 and environmental isolates) on mineral surfaces.* Environmental Science & Technology, 2005. **39**(17): p. 6395-6404.

108. Vanoss, C.J., *ACID-BASE INTERFACIAL INTERACTIONS IN AQUEOUS-MEDIA.* Colloids and Surfaces a-Physicochemical and Engineering Aspects, 1993. **78**: p. 1-49.

109. Butt, H.J., B. Cappella, and M. Kappl, *Force measurements with the atomic force microscope: Technique, interpretation and applications.* Surface Science Reports, 2005. **59**(1-6): p. 1-152.

110. Neidhardt, F.C., Curtiss, R., III, Ingraham, J. L., Lin, E. C. C., Low, K. B., Magasanik, B., Reznikoff, W. S., Riley, M., Schaechter, M., Umbarger, H. E., Eds.;, *Escherichia coli and Salmonella: cellular and molecular biology*. 2nd ed ed1996, Washington, D. C.: ASM Press.

111. Haznedaroglu, B.Z., C.H. Bolster, and S.L. Walker, *The role of starvation on Escherichia coli adhesion and transport in saturated porous media.* Water Research, 2008. **42**(6-7): p. 1547-1554.

112. Morel, F.H., J. G., *Principles and Applications of Aquatic Chemistry*. Vol. xv. 1993, New York: Wiley.

113. Kim, H.N., S.A. Bradford, and S.L. Walker, *Escherichia coli O157:H7 Transport in Saturated Porous Media: Role of Solution Chemistry and Surface Macromolecules.* Environmental Science & Technology, 2009. **43**(12): p. 4340-4347.

114. Hogg, R.H., T. W.; Fuerstenau, D. W. T., Faraday Soc., 1966. **62, 1638-1651**.

APPENDIX: Figures from previous work

Breakthrough curves of *E. coli* O157 in10mM Ionic Strength Solution

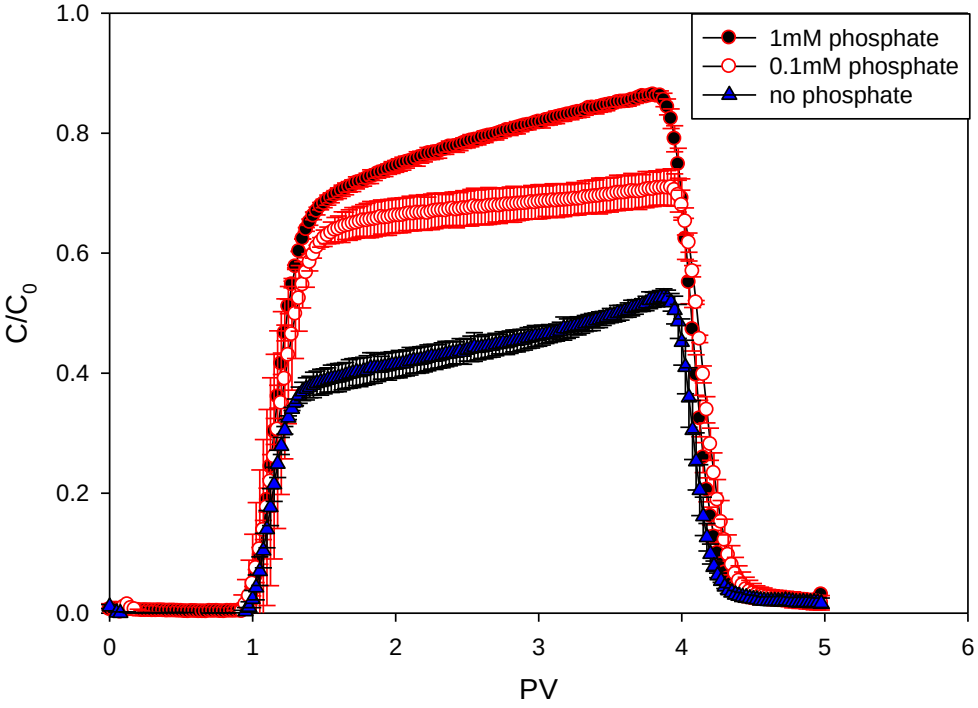

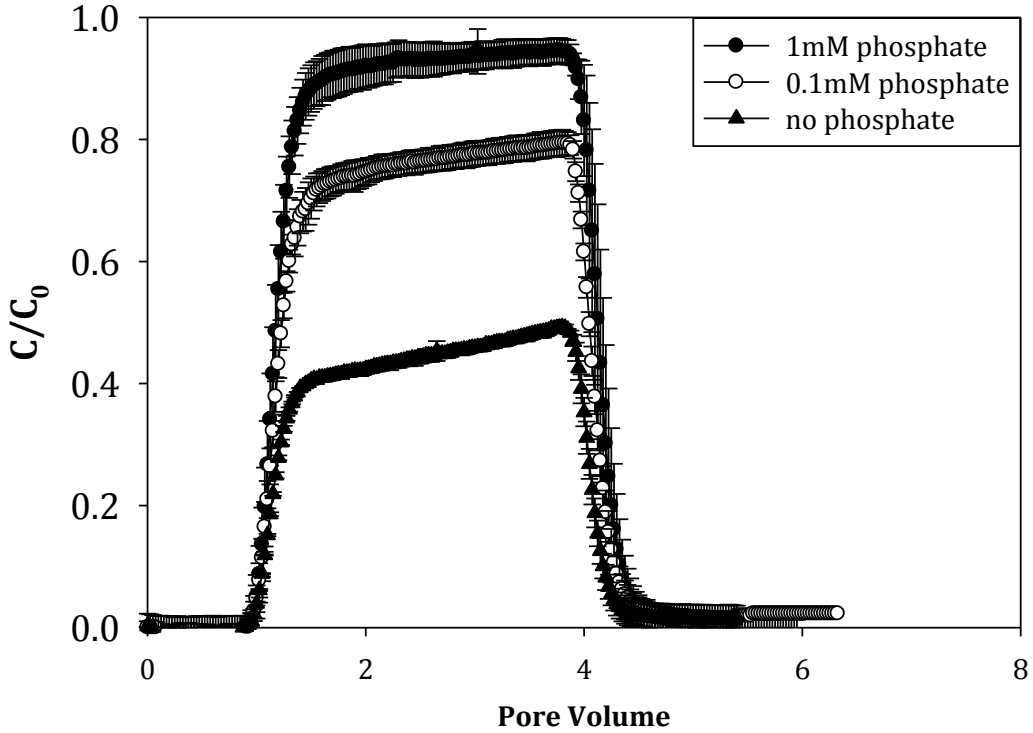

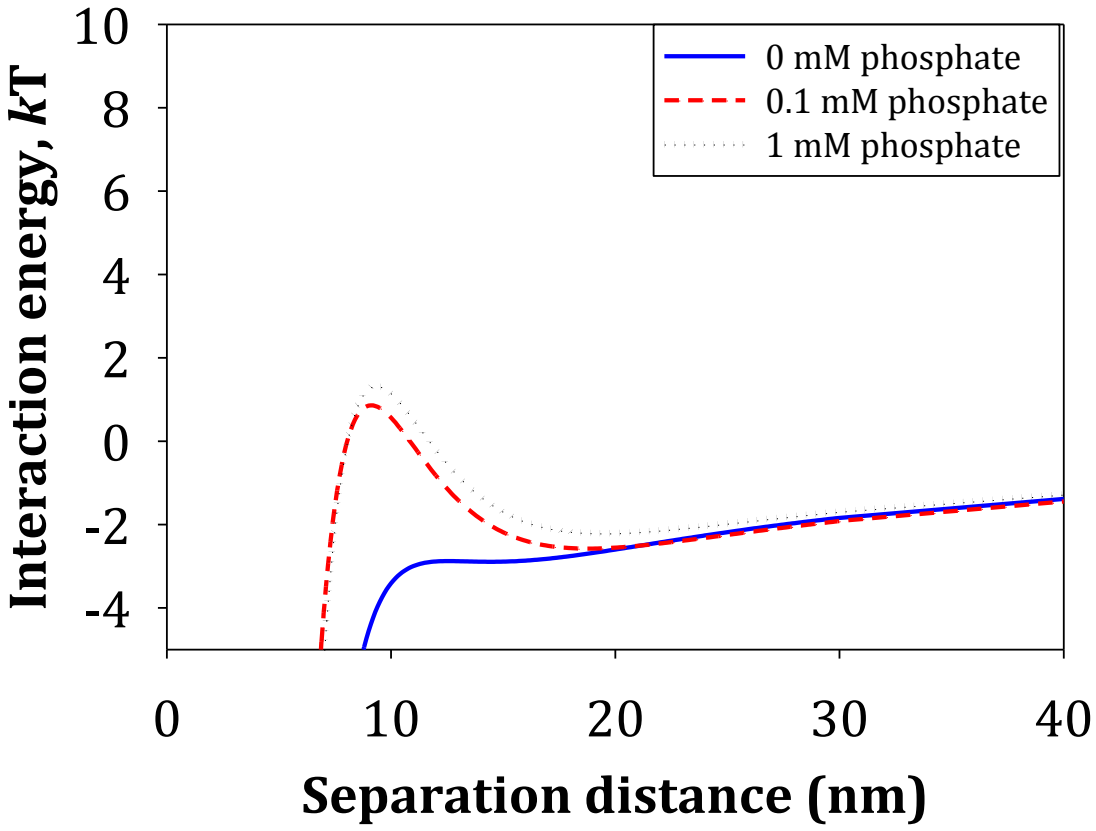
Interaction energy, kT
10
8
6
4
2
0
-2
-4
0 mM phosphate
0.1 mM phosphate
1 mM phosphate
0
10
20
30
40
Separation distance (nm)

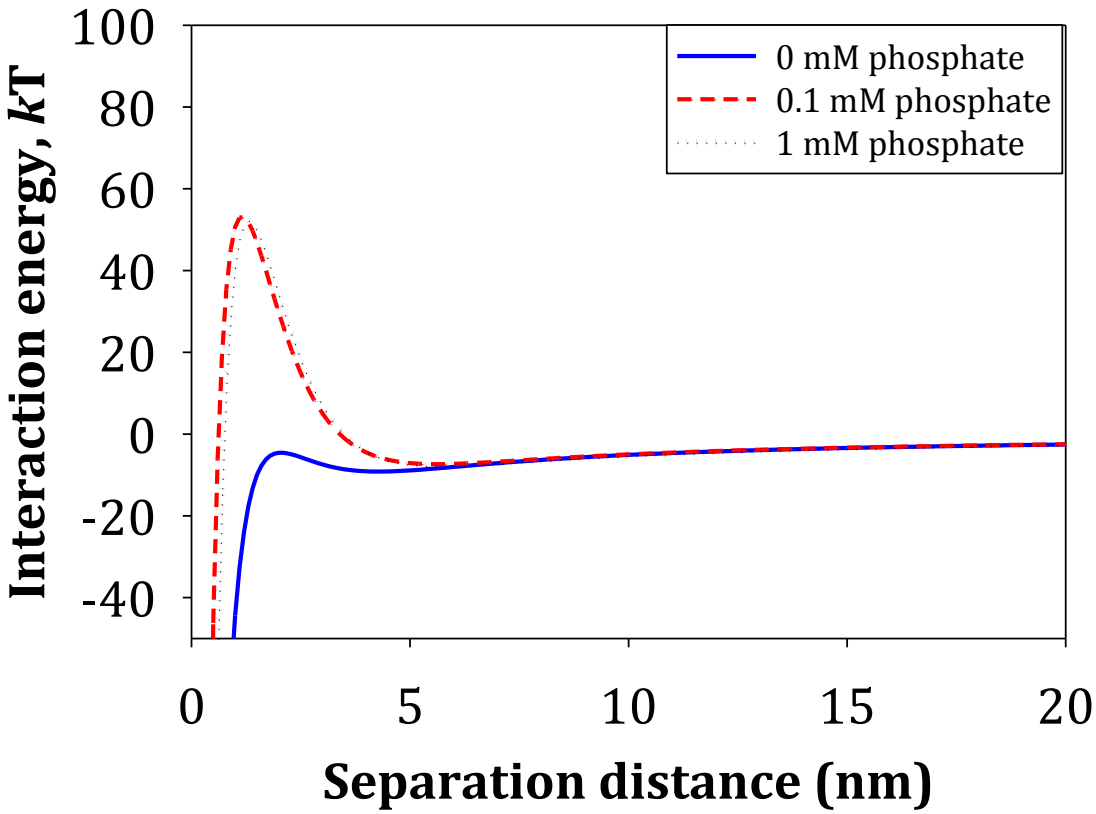
Interaction energy, kT
100
80
60
40
20
0
-20
-40
0 mM phosphate
0.1 mM phosphate
1 mM phosphate
0
5
10
15
20
Separation distance (nm)

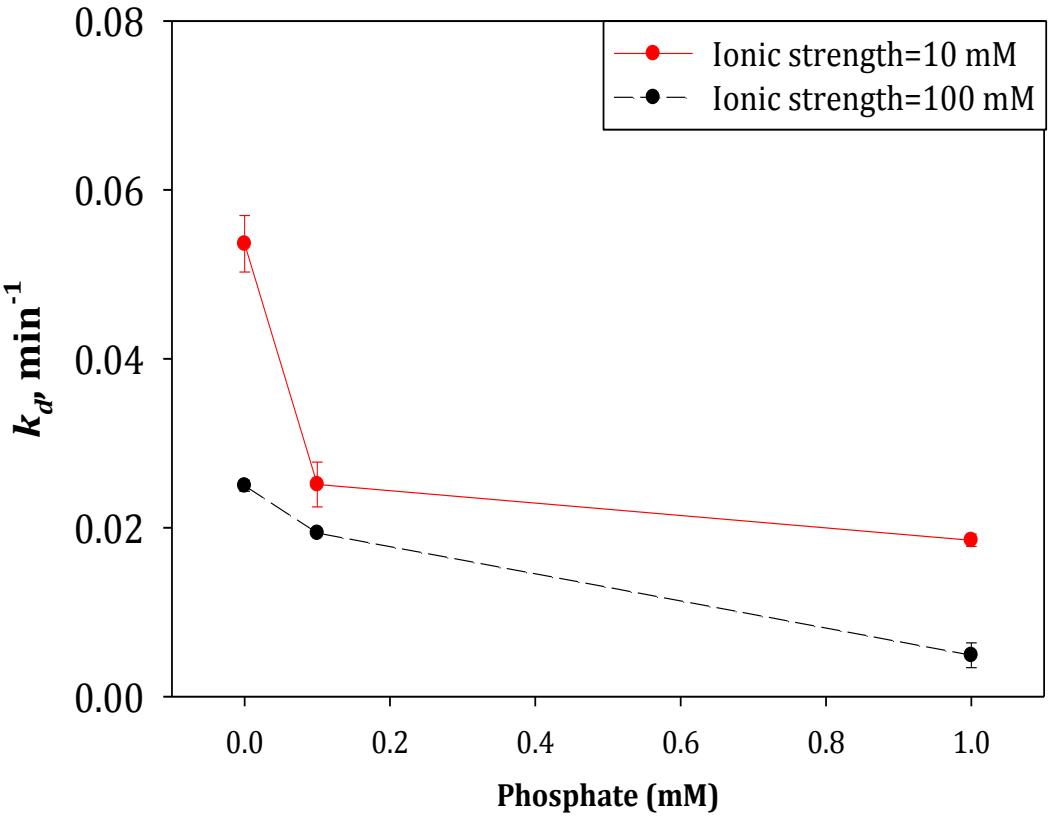
0.08
0.06
0.04
0.02
0.00
k_d, min^{-1}
Ionic strength=10 mM
Ionic strength=100 mM
0.0
0.2
0.4
0.6
0.8
1.0
Phosphate (mM)

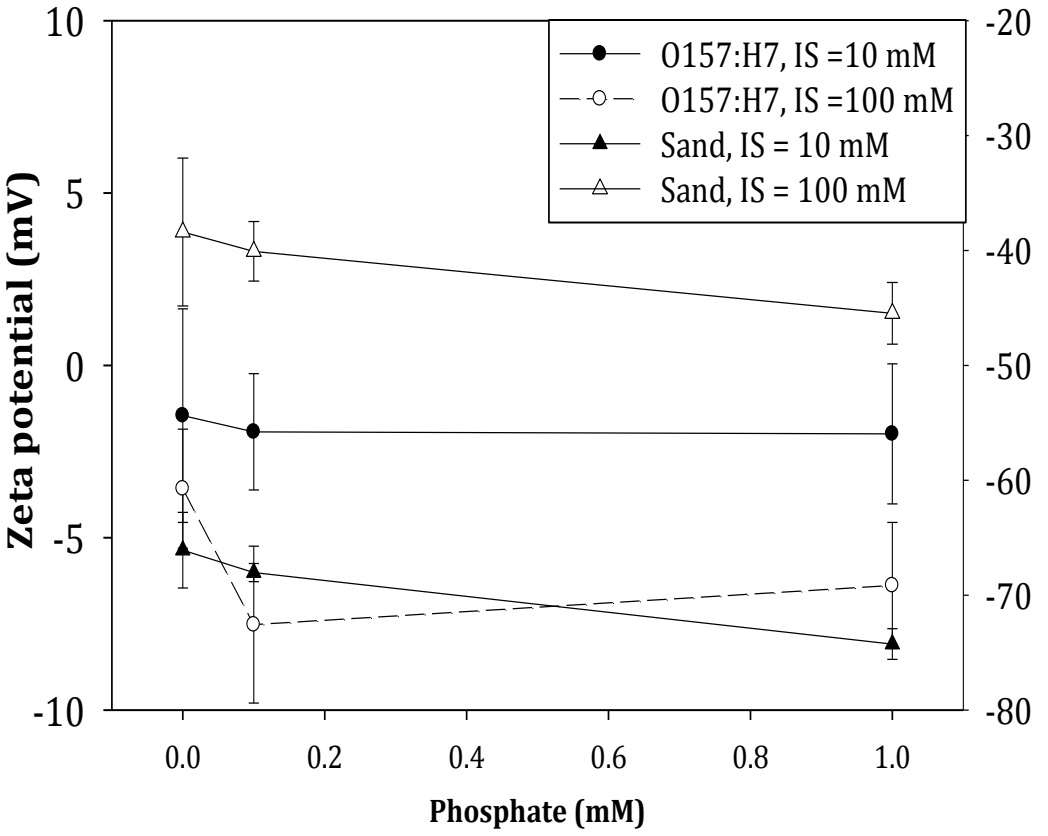
10
5
0
-5
-10
Zeta potential (mV)
-20
-30
-40
-50
-60
-70
-80
O157:H7, IS =10 mM
O157:H7, IS =100 mM
Sand, IS = 10 mM
Sand, IS = 100 mM
0.0
0.2
0.4
0.6
0.8
1.0
Phosphate (mM)